Article:
Pearson, Caroline, Tindall, Sarah, Herman, Reyme et al. (5 more authors) (2020) Acetylation of surface carbohydrates in bacterial pathogens requires coordinated action of a two-domain membrane-bound acyltransferase. MBio. e01364-20. pp. 1-19. ISSN 2150-7511

https://doi.org/10.1128/mBio.01364-20

Acetylation of surface carbohydrates in bacterial pathogens requires coordinated action of a two-domain membrane-bound acyltransferase

Caroline R Pearson[a,b,1]; Sarah N Tindall [a,b,1]; Reyme Herman[b]; Huw T Jenkins[d]; Alex Bateman[e], Gavin H Thomas[a,b], Jennifer R Potts[b]; Marjan W Van der Woude[a,c]

Author Affiliation:
a York Biomedical Research Institute, University of York, York YO10 5DD, UK
b Department of Biology, University of York, York YO10 5DD, UK
c Hull York Medical School, University of York, York YO10 5DD, UK
d York Structural Biology Laboratory, Department of Chemistry, University of York, York YO10 5DD, UK
e European Molecular Biology Laboratory, European Bioinformatics Institute (EMBL-EBI), Wellcome Genome Campus, Hinxton, Cambridgeshire CB10 1SD, UK

Corresponding Author: M. W. Van der Woude; York Biomedical Research Institute and Hull York Medical School; Wentworth Way; University of York, Heslington, York YO10 5DD; United Kingdom

email: Marjan.vanderwoude@york.ac.uk

[1] Caroline R. Pearson and Sarah N. Tindall contributed equally to this work. Author order was determined alphabetically.

Abstract

Membrane bound Acyltransferase_3 (AT3) domain-containing proteins are implicated in a wide range of carbohydrate *O*-acyl modifications but their mechanism of action is largely unknown. O-antigen acetylation by AT3 domain-containing acetyltransferases of *Salmonella* spp. can generate a specific immune response upon infection and can influence bacteriophage interactions. This study integrates *in situ* and *in vitro* functional analysis of two of these proteins, OafA and OafB (formerly F2GtrC) which display an 'AT3-SGNH fused' domain architecture where an integral membrane AT3 domain is fused to an extra-cytoplasmic SGNH domain. An *in silico*-inspired mutagenesis approach of the AT3 domain identified seven residues which are fundamental for the mechanism of action of OafA, with a particularly conserved motif in TMH1 indicating a potential acyl donor interaction site. Genetic and *in vitro* evidence demonstrates that the SGNH domain is both necessary and sufficient for lipopolysaccharide acetylation. The structure of the periplasmic SGNH domain of OafB identified features not previously reported for SGNH proteins. In particular, the periplasmic portion of the inter-domain linking region is structured. Significantly, this region constrains acceptor substrate specificity, apparently by limiting access to the active site. Co-evolution analysis of the two domains suggests possible inter-domain interactions. Combining these data we propose a refined model of the AT3-SGNH proteins, with structurally constrained orientations of the two domains. These findings enhance our understanding of how cells can transfer acyl groups from the cytoplasm to specific extracellular carbohydrates.

Importance

Acyltransferase-3 (AT3) domain-containing membrane proteins are involved in O-acetylation of a diverse range of carbohydrates across all domains of life. In bacteria they are essential in processes including symbiosis, resistance to antimicrobials, and biosynthesis of antibiotics. Their mechanism of action, however, is poorly characterised. We analysed two acetyltransferases as models for this

important family of membrane proteins, that modify carbohydrates on the surface of the pathogen *Salmonella enterica*, affecting immunogenicity, virulence and bacteriophage resistance. We show that when these AT3 domains are fused to a periplasmic partner domain, both domains are required for substrate acetylation. The data shows conserved elements in the AT3 domain and unique structural features of the periplasmic domain. Our data provides a working model to probe the mechanism and function of the diverse and important members of the widespread AT3 protein family, which are required for biologically significant modifications of cell-surface carbohydrates.

Introduction

Salmonella infections are a considerable public health burden in both developing and developed countries. *Salmonella enterica* subspecies *enterica* serovar Typhimurium (STM) is estimated to cause more than 150,000 human deaths from gastroenteritis each year (1, 2). A sublineage of this serovar is the dominant cause of invasive non-Typhoidal *Salmonella* (iNTS) bloodstream infections in Africa (3). The Typhi serovar of this subspecies is the major cause of typhoid fever, resulting in over 200,000 deaths annually (2, 4). In the US, there are over 10,000 cases annually of these serovars combined (5, 6).

Cell surface lipopolysaccharide (LPS) is an important virulence factor. The O-antigen, the most distal and variable portion of LPS, is composed of repeating oligosaccharide units whose composition and structure varies between species and, in the case of *Salmonella* spp., between serovars. Modification of the O-antigen by alteration of sugar linkages or addition of moieties such as glucose or acetate (7, 8) can influence immunogenicity, virulence, and confer resistance to lytic phage infection (9–12).

Carbohydrates on the bacterial cell surface are frequently O-acetylated by acyltransferase proteins which contain a 10 transmembrane helix (TMH) Acyltransferase_3 (AT3, IPR002656, PF01757; also

70 known as Acyltransferase_3/Putative Acetyl-CoA Transporter, TC 9.B.97). This family of proteins is
71 widespread in eukaryotes and prokaryotes and is involved in a range of acylation modifications.
72 Examples of AT3-containing acetyltransferases from prokaryotes include those mediating
73 peptidoglycan acetylation contributing to lysozyme resistance (13, 14), modification of root
74 nodulation factors to initiate symbioses (15), and O-antigen acetylation (9, 16, 17). Despite the
75 involvement of AT3-containing proteins in a wide range of reactions, their mechanism and structure
76 are poorly characterised.

77 Among bacterial AT3 carbohydrate acetyltransferases, there are two known domain architectures;
78 proteins consisting of an AT3 domain only (AT3-only) and an N-terminal AT3 domain linked to an
79 extra-cytoplasmic domain, commonly an SGNH domain (AT3-SGNH fused). The SGNH domain is
80 fused through addition of an 11th TMH and linking region. Oac (in *Shigella* spp.) is an example of an
81 AT3-only protein that is essential for O-antigen acetylation (18) whereas OatA, the O-
82 acetyltransferase of peptidoglycan in *Staphylococcus* spp., is an example of an AT3-SGNH fused
83 protein (14). SGNH domains (InterPro IPR036514) are a large and diverse family of small catalytic
84 domains of around 200 amino acids, originally characterised as a subgroup of the GDSL hydrolase
85 family by their particular invariant residues, Ser, Gly, Asn, His - hence SGNH – which occur in four
86 blocks of conserved sequence (19, 20). Members of this family that are active against carbohydrates
87 are also classified as CE3 family proteins in CAZy (21). Subsequently, many more proteins have been
88 found to belong to this diverse family and they no longer fully adhere to the original paradigm of
89 SGNH. However, most members typically contain a catalytic triad of Ser, His, Asp and oxyanion hole
90 residues within the four blocks of conserved sequence (22). It is not clear how the AT3 and SGNH
91 domains function together in AT3-SGNH fused carbohydrate acetyltransferases, nor how the AT3-
92 only proteins function independently of a linked periplasmic domain.

93 In *Salmonella* spp. there are two defined O-antigen acetyltransferases OafA and OafB (9, 10, 17, 23).
94 Slauch *et al.* determined that the integral membrane protein OafA from STM (17), acetylates the 2-

95 hydroxyl group on the abequose moiety of the O-antigen unique to this serovar (24). This results in
96 acquisition of the O:5 serotype (defined by the Kauffmann White Lee Minor scheme) (25, 26) which
97 is required for production of protective antibodies against STM infection (24, 27). Multiple
98 *Salmonella* serovars have a rhamnose moiety in the O-antigen that can be acetylated at the 2- and 3-
99 hydroxyl groups by F2GtrC proteins (9, 10, 23). As it is clear that F2GtrC is an acetyltransferase with
100 no functional relationship to the GtrABC glycosylating proteins, we propose to rename this and
101 orthologous rhamnose acetyltransferases as OafB. The name reflects the protein architecture (O-
102 antigen acetyltransferase fused B), similar to that we suggest for OafA (O-antigen acetyltransferase
103 fused A).

104 In this work, using *in situ* and *in vitro* functional analysis of OafA and OafB O-antigen
105 acetyltransferases, we address the following key questions to further our understanding of the
106 mechanism of acetyl transport and transfer in AT3-SGNH fused acetyltransferases. (I) Are there
107 essential residues in the membrane-bound AT3 domain that can give clues to their role in acetyl
108 transfer? (II) Can we obtain insight into the architecture of these proteins by elucidating the
109 structure of the SGNH domain and its N-terminal extension? (III) What is the function of the SGNH
110 domain and can it function independently of the AT3 domain?

111

112 # Results

113 ## *In silico* analysis identifies conserved features in the integral membrane domains of
114 bacterial AT3 acetyltransferases

115 The STM O-antigen acetyltransferases OafA (17) and OafB (23) (formerly F2GtrC) are both predicted
116 by InterPro to contain an N-terminal AT3 domain (IPR002656, PF01757) fused to an SGNH domain
117 (IPR013830, PF14606 or PF13472) (28, 29) (Fig. 1*A*). The AT3 domain has 10 TMH and an additional

118 11th helix that is presumably required to localise the fused SGNH domain in the periplasm (Fig. 1*A*)
119 (30); this prediction is supported by experimental topology analysis of OafB (9) and consistent with
120 topology analysis of Oac (31) , a comparison enabled by our detailed alignments (see below).
121 Reinforcing the widespread functions of these understudied proteins in bacteria, we identified in the
122 literature 30 bacterial AT3 domain-containing proteins, with experimentally confirmed carbohydrate
123 acetyltransferase activity (9, 14–17, 32–55). Of these 30 proteins, 19 contain just the AT3 domain,
124 while 11, including OafA and OafB, have the fused AT3-SGNH architecture (*SI Appendix,* Table S1).
125 Previous work showed that in OafA and OafB, the SGNH domain is essential for acetyltransferase
126 activity (9, 56) and thus, we propose the following working model for the mechanism of action (Fig.
127 1*B*). In AT3-SGNH proteins, the AT3 domain passes an acetyl group from an unidentified donor in the
128 cytoplasm to the periplasmic face of the inner membrane. This acetyl group is then transferred to
129 the SGNH domain, which catalyses specific carbohydrate O-acetylation (Fig. 1*B*). To test this model,
130 we first determined whether residues conserved between AT3-only and AT3-SGNH
131 acetyltransferases are important for acetyltransferase activity.

132 Alignments of the 30 characterised AT3 acetyltransferases along with a *S. enterica* serovar Paratyphi
133 A (SPA) OafB homologue revealed that only 4 amino acids are invariant across all 31 proteins,
134 $OafA_{H25}$, $OafA_{F41,}$ $OafA_{G46}$ and $OafA_{G202}$ (Fig. 2*A*, *SI Appendix,* Fig. S1). $OafA_{F41}$ and $OafA_{G46}$ belong to
135 the FFXISG motif previously identified in un-fused AT3 O-antigen acetyltransferases (*SI Appendix,* Fig.
136 S1) (31). Two conserved residues are predicted in TMH1, separated by 10 amino acids, in an R/K-X_{10}-
137 H motif (Fig. 2*A*, *SI Appendix,* Fig. S1). A previously identified RXXR motif ($OafA_{R69,R72}$) in loop 2-3 is
138 essential for activity in *Shigella flexneri* Oac ($Oac_{R73,\ R75}$)(57), and OafB ($OafB_{R71,\ R73}$) (9). This motif is
139 highly (but not absolutely) conserved across the 31 analysed acetyltransferases.

140 We next examined features unique to the AT3 domains of AT3-SGNH fused acetyltransferases; these
141 11 sequences derive from diverse Gram positive and Gram negative bacteria (Fig. 2*B*, *SI Appendix,*
142 Table S1). The most striking shared feature of AT3-SGNH fused proteins is the highly conserved GG-

143 F/Y-XGV-D/P/V motif located at the periplasmic side of TMH2 ($OafA_{G33-D39}$), which replaces a longer
144 and more divergent loop region between TMH1-2 in the non-fused AT3 proteins. Further conserved
145 residues are seen in the periplasmic loop between TMH3-4, including $OafA_{S112}$, $OafA_{N113}$ and $OafA_{Y122}$.
146 Together these observations suggest shared key residues in both AT3-only and AT3-SGNH fused
147 proteins and possible adaption of AT3 domains in AT3-SGNH fused acetyltransferases towards their
148 function together with the fused SGNH domain.

149 Site-directed mutagenesis combined with *in situ* functional analysis of OafA 150 identifies functional residues within the AT3 domain

151 To determine the functional importance of conserved residues in $OafA_{STM}$, we developed an *in situ*
152 functional assay using a double antibody LPS immunoblot. The assay quantifies both the level of
153 acetylated abequose (O:5) and the amount of LPS based on the O-antigen core (Fig. 3). His-tagged
154 OafA, or mutated versions thereof, were expressed *in trans* in a strain that lacks all O-antigen
155 modification genes including *oafA* (strain 293) (Methods, *SI Appendix,* Table S2). Levels of abequose
156 acetylation in these strains was determined by LPS immunoblot from the signal obtained with
157 serotype antibody and protein expression was also confirmed (Fig. 3, *SI Appendix,* Fig. S2). We
158 validated this approach by comparing abequose acetylation by the *in trans* system, to both
159 chromosomal His-tagged OafA and wild type OafA. This showed that despite a higher level of
160 protein in the *in trans* system (Fig. 3*B*), a comparable level of abequose acetylation was obtained in
161 all strains (Fig. 3*A* and *SI Appendix,* Fig. S2).

162 Twenty positions in the membrane bound domain of OafA were individually engineered to replace
163 the wild-type amino acid with alanine. The level of O-antigen acetylation *in situ* as a result of mutant
164 protein expression is summarized in Table 1 and Fig. 4, and data are shown in *SI Appendix,* Fig. S2.
165 Point mutants that gave <1% O-antigen acetylation signal in relation to wild type were considered to
166 be inactive and those with <50% O-antigen acetylation signal were considered to have significantly

167 reduced activity. For all mutant proteins except G34A there was detectable full-length protein on the
168 Western blot, sometimes in addition to degradation products (*SI Appendix,* Fig. S2). Assay validation
169 experiments indicate that the levels of full length mutant protein is in excess of wild type levels and
170 thus should be sufficient to confer detectable abequose O-acetylation.

171 The arginine and histidine residues in the R/K-X_{10}-H motif ($OafA_{R14}$ and $OafA_{H25}$) are essential for
172 function. These residues are predicted to be on the same surface of the alpha helix with a spacing
173 similar to the predicted distance between the 3' phosphate and the thioester bond of one coenzyme
174 A molecule (~19 Å). Thus, we hypothesise these residues provide a potential Acetyl-CoA interaction
175 site within the AT3 domain. The 100% conserved glycines ($OafA_{G46}$ and $OafA_{G202}$) could be replaced
176 with alanine with no detriment. As expected, both arginines in the TMH3 RXXR motif ($OafA_{R69, R72}$) (9,
177 57) were essential for OafA function (Table 1, Fig. 4).

178 We next examined the unique aspects of the AT3 domains among the AT3-SGNH fused proteins. Of
179 the conserved GG-F/Y-XGV-D/P/V motif and flanking residues, mutation of $OafA_{F35}$ and $OafA_{D39}$
180 caused significant reduction and complete loss of OafA activity, respectively. $OafA_{S112A}$ mutation also
181 caused complete loss of OafA activity (Table 1, Fig. 4). AT3-only acetyltransferases do not contain an
182 11th TMH but a glutamate residue after the C-terminal end of TMH10 ($OafA_{E325}$) is invariant across
183 AT3-SGNH protein sequences; mutation of this residue ($OafA_{E325A}$) resulted in significant reduction in
184 OafA activity (Table 1, Fig. 4). Thus, AT3-SGNH-specific conserved residues in the AT3 domain are
185 inherently involved in the mechanism of action of OafA.

186 $OafB_{SPA}^{long}$ has an extended SGNH-like fold

187 To gain an understanding of the mechanism of OafA and OafB both domains must be analysed, thus
188 *in vitro* analysis of the SGNH domain was conducted. Structural analysis of the SGNH domains and
189 periplasmic linking regions of OafA and OafB were used to gain insight into the functional
190 adaptations of an SGNH domain fused directly to an AT3 domain. We expressed and purified

191 residues 366 to 609 from OafA ($OafA_{STM}^{C\text{-}long}$) and residues 377 to 640 of SPA OafB from ($OafB_{SPA}^{C\text{-}long}$), which have 31% sequence identity (Fig. 1*A*). Although $OafB_{SPA}$ has not been experimentally characterised in the literature, SPA O-antigen rhamnose can be acetylated (58) and $OafB_{SPA}$ has 78% sequence identity to the experimentally characterised $OafB_{STM}$ rhamnose acetyltransferase (9).

195 No diffracting crystals of $OafA_{STM}^{C\text{-}long}$ could be obtained, however, crystals diffracting to 1.1 Å resolution were obtained for $OafB_{SPA}^{C\text{-}long}$, with a single molecule in the asymmetric unit. The structure could not be solved by molecular replacement using a number of known SGNH structures, but was solved using Fragon (59) with a 14 residue ideal polyalanine α-helix as the search model and refined to an R_{work}/R_{free} of 13.6/14.9% (*SI Appendix,* Table S3).

200 The core structure of $OafB_{SPA}^{C\text{-}long}$ resembles an SGNH domain, with an α/β/α hydrolase fold consisting of five central β-strands surrounded by six α-helices (Fig. 5*A*). Two disulfide bonds are seen in the structure (Fig. 5*A*) and were verified using mass spectrometry. The closest structural homologues to $OafB_{SPA}^{C\text{-}long}$, as identified by the DALI server, are carbohydrate esterases from *Talaromyces cellulolyticus* (5B5S) and *Clostridium thermocellum* (2VPT); each have an RMSD of 2.5 Å over 207 and 201 backbone residues, respectively.

206 The first clear difference between $OafB_{SPA}^{C\text{-}long}$ when compared to its closest structural homologues and the only other SGNH domain from a fused acyltransferase with a solved crystal structure, OatA-SGNH (5UFY) (60) is that the structure is significantly larger, at ~36k $Å^3$, compared to OatA-SGNH at ~23k $Å^3$, which is more similar to the size of the two most closely related structures of the carbohydrate esterases (2VPT is ~26k $Å^3$ and 5B5S is 27k $Å^3$). This additional volume in the fold is contributed by two separate non-contiguous parts of the structure, the first being helix α8, which comprises 10% of the SGNH domain volume (Fig. 5). A structure-based alignment of related SGNH domains indicated that the sequence forming this additional helix is only present in AT3-SGNH domains involved in acetylation of LPS O-antigens (Fig. 6A*, SI Appendix,* Fig. S3) and so is missing on OatA. Secondly, and most significantly the region that connects the end of TM11 and the start of the

216 sequence of other known SGNH domains (residues 377-421) is clearly structured and forms a long
217 extension of the SGNH domain that we now term the SGNH extension ($SGNH_{ext}$). The $SGNH_{ext}$
218 interacts extensively with the SGNH domain covering 1500 $Å^2$ of the SGNH domain, including
219 interactions with helix α8; 38 amino acids of the SGNH domain interact with 32 (of 48) residues in
220 the extension. Removal of the most N-terminal half of the $SGNH_{ext}$ ($OafA_{STM}^{C\text{-}short}$ and $OafB_{SPA}^{C\text{-}short}$
221 (Fig. 1A)), results in a decrease in melting temperature of 5.7 ^{o}C in OafA and 8.9 ^{o}C in OafB
222 suggesting that the $SGNH_{ext}$ has a stabilising effect on the SGNH domain (*SI Appendix,* Fig. S4). These
223 observations show that $OafB_{SPA}^{C\text{-}long}$ forms an extended SGNH-like fold with an additional helix, and
224 the periplasmic portion of the linking region is structured and interacts with the SGNH domain.

225 Catalytic residues of $OafB_{SPA}^{long}$ resemble a typical SGNH domain with an atypical 226 oxyanion hole

227 SGNH domains are usually characterised by the presence of four blocks of sequence, containing
228 conserved residues: block I – GDS, block II – G, block III – GxND and block V – DxxH (where x is any
229 non-proline residue) (22). The structure-based sequence alignment was used to identify conserved
230 residues in the SGNH domain of fused acyltransferases (Fig. 6*B, SI Appendix,* Fig. S3). The typical
231 SGNH catalytic triad, consisting of serine (block I), aspartic acid and histidine (block V), is conserved
232 in the sequence of both OafA and OafB. *In situ* functional analysis of catalytic triad mutants $OafA_{S412A}$
233 and $OafA_{H590A}$ showed almost complete loss of function, whereas $OafA_{D587A}$ showed reduced activity
234 (Table 2, Fig. S2). This is consistent with analyses of typical catalytic triad activity in other SGNH
235 proteins (61, 62).

236 While the catalytic triad is conserved in both proteins, the oxyanion hole residues, glycine (block II)
237 and asparagine (block III), are not (Fig. 6*B*). Analysis of the structure-based alignment of the block II
238 region (Fig. 6*B, SI Appendix,* Fig. S3) reveals the conserved glycine is replaced by an asparagine in
239 OafB ($OafB_{N459}$). The structure of $OafB_{SPA}^{C\text{-}long}$ shows $OafB_{N459}$ to be within hydrogen bonding distance
240 of a co-crystallised sulfate ion (Fig. 6*C*) suggesting that $OafB_{N459}$ could interact with bound substrate

241 and participate in oxyanion hole formation. Homology modelling of $OafA_{STM}^{C\text{-}long}$ based on the
242 structure of $OafB_{SPA}^{C\text{-}long}$ (*SI Appendix,* Fig. S5) suggests that the $OafA_{S437}$ side chain or $OafA_{L438}$ are
243 most likely to replace the block II glycine in the oxyanion hole. This was supported by the *in situ*
244 abequose acetylation assay which shows $OafA_{S437A}$ has significantly reduced activity in comparison to
245 wild type OafA (Table 2, Fig. S2) consistent with the decrease in activity seen on mutation of the
246 oxyanion hole residues in other SGNH domains (60, 61, 63)**.**

247 The GxND motif (block III), where Asn is typically involved in oxyanion hole formation (20), is not
248 evident in OafA or OafB in the structure-based alignment (Fig. 6*B*). $OafB_{SPA}^{C\text{-}long}$ contains a GTNG
249 motif ($OafB_{G502\text{-}G505}$) close to sequence block III (Fig. 6*B*)**,** but the side chains of these residues are
250 oriented away from the catalytic triad (Fig. 6*C*). These observations suggest that**,** although OafA and
251 OafB display the typical catalytic triad of an SGNH domain, their oxyanion hole arrangement is
252 atypical.

253 The $SGNH_{ext}$ confers acceptor specificity

254 The structured region that extends the OafB SGNH domain ($SGNH_{ext}$) appears to occlude the active
255 site and results in significantly lower solvent accessible surface area (SASA) of the catalytic triad
256 residues (40 Å) than in OatA, 2VPT and 5B5S (132 Å, 110 Å and 126 Å, respectively) (Fig. 5*C*).
257 Removing the 22 most N-terminal residues from the structure of $OafB_{SPA}^{C\text{-}long}$ ($OafB_{SPA}^{C\text{-}short}$, Fig. 1*A*)
258 increases the SASA of the catalytic triad residues of OafB to 107.9 Å.

259 To assess the potential consequences of an occluded active site for substrate specificity, assays were
260 carried out for OafA and OafB containing the full $SGNH_{ext}$ ($OafA_{STM}^{C\text{-}long}$ and $OafB_{SPA}^{C\text{-}long}$) and those
261 with half the $SGNH_{ext}$ ($OafA_{STM}^{C\text{-}short}$ and $OafB_{SPA}^{C\text{-}short}$) (Fig. 1*A*). *In vitro* catalytic activity was first
262 confirmed for all constructs via their ability to hydrolyse the ester substrate p-nitrophenyl acetate
263 (pNP-Ac) (*SI Appendix,* Fig. S6), an assay commonly used to test SGNH domain function (64, 65). This

264 activity suggests that all four proteins are correctly folded and catalytically active regardless of the
265 presence or absence of the $SGNH_{ext}$ residues covering the active site (*SI Appendix,* Fig. S6).

266 To assess whether $SGNH_{ext}$ affects the *in vitro* acceptor substrate specificity of $OafA_{STM}^{C\text{-}term}$ and
267 $OafB_{SPA}^{C\text{-}term}$ proteins, purified proteins were incubated with pNP-Ac (acetyl group donor) and
268 unmodified STM LPS (Path993, *SI Appendix,* Table S2) as the acceptor substrate, and O:5 antibodies
269 were used to probe for O-antigen abequose acetylation. Abequose is the native acceptor sugar for
270 OafA whereas OafB acetylates rhamnose *in situ*. A positive signal for O:5 antibody binding is gained
271 after incubation with $OafA_{STM}^{C\text{-}long}$ and $OafA_{STM}^{C\text{-}short}$ (Fig. 7). Thus, $OafA_{STM}^{C\text{-}long}$ and $OafA_{STM}^{C\text{-}short}$ are
272 able to acetylate their native substrate in solution. In contrast, acetylation of the non-native
273 acceptor substrate by OafB occurs only in the absence of the OafB $SGNH_{ext}$ ($OafB_{SPA}^{C\text{-}short}$) (Fig. 7).
274 Firstly, these results support our working model that the SGNH domain performs the last step in the
275 transferase reaction; the transfer of the acetyl moiety to the acceptor carbohydrate. Furthermore,
276 these results strongly indicate that the acceptor substrate specificity of this SGNH domain is
277 constrained by the cognate, structured $SGNH_{ext}$.

278 Evolutionary support for an interaction between the AT3 domain and the SGNH 279 domain

280 The discovery that the 'linker' region that is present between the more clearly defined AT3 and
281 SGNH domains is in fact a long structured component of the SGNH domain, means that the SGNH is
282 much more constrained and proximal to the membrane that initially proposed if this region was a
283 long flexible linker. The discovery that there are residues in the AT3 loop between TMH3-4 that are
284 only conserved in the AT3-SGNH fused proteins, suggests potential protein-protein contacts
285 between the two domains during catalysis. To test this hypothesis we used a co-evolution analysis of
286 the OafA-B type acetyltransferases to assess whether there was any evidence for correlated changes
287 in the two domains consistent with a physiological interaction (Fig. S7a). While there are many
288 correlated changes within the two separate domains, a significant correlated changes was observed

289 between residues 95 and 97, located in the periplasmic loop between TMH3-4 of the AT3 domain
290 (Fig. 8) and residues 542 and 545-546, which form a surface-accessible patch (Fig. S7b) on the
291 additional helix (α8) of the SGNH domain (Fig. 8). This predicted interaction further informs our
292 refined topological model of these AT3-SGNH acetyltransferases (Fig. 8).

293 Discussion

294 AT3 domain-containing proteins (PF01757) are a ubiquitous family of proteins involved in diverse
295 carbohydrate modifications across the domains of life. Prokaryotic members of this family play roles
296 in modification of antibiotics and antitumor drugs, as well as initiation of microbial symbioses with
297 plants (15, 66, 67)(*SI Appendix,* Table S1). In bacterial pathogens, such as *Salmonella enterica*,
298 *Listeria monocytogenes*, *Haemophilus influenzae* and *Streptococcus pneumonia*, these proteins are
299 implicated in acetylation of extra-cytoplasmic polysaccharides which can have significance for
300 interactions with phage and hosts and can affect virulence and antibiotic resistance (24, 32, 36, 38).
301 The current experimentally characterised AT3 domain-containing carbohydrate O-acetyltransferases
302 display SGNH-fused or AT3-only domain architecture. Although both AT3 and SGNH domains display
303 broad substrate ranges in diverse biological systems, the mechanism of action of both SGNH-fused
304 and AT3-only acetyltransferases is largely unknown.

305 Previous understanding of AT3-SGNH fused acetyltransferases was obtained by *in situ* functional
306 assays, and structure-function assessment of the SGNH domain (9, 17, 60). Here, expanded
307 bioinformatic analysis with a set of 30 experimentally characterised bacterial AT3 acetyltransferases,
308 including AT3-only and AT3-SGNH fused protein sequences, which perform a range of biological
309 functions (*SI Appendix,* Table S1), revealed commonalities and key differences. For example, an R/K-
310 X_{10}-H motif in TMH1 is shared across all the bacterial AT3 acetyltransferases studied (Fig. 2) and is
311 also highly conserved across all AT3 domain proteins in the Pfam database (29), strongly suggesting
312 that these are critical catalytic residues relevant to the whole protein family.

313 $OafA_{R14}$ and $OafA_{H25}$ within this motif were essential for activity (Table 1, Fig. 4) and are predicted to
314 be at opposite ends, but on the same surface, of the TMH1 helix (arginine towards the cytoplasmic
315 side) providing a potential interaction site for the proposed acetyl group donor acetyl-CoA. Although
316 cytoplasmic acetyl-CoA has not been confirmed as the donor for O-antigen acetylation, it occupies a
317 central role in bacterial metabolism and is a prominent source of acetate in bacterial cells (68, 69).
318 Arginine residues have previously been implicated in binding of the 3' phosphate of acetyl-CoA in
319 other acetyltransferase proteins (70) and conserved histidine residues in the soluble mitochondrial
320 carnitine O-acyltransferase co-ordinate the thioester bond of acyl-CoA with the carnitine acceptor to
321 catalyse the acyl-transfer reaction (71). Significantly the equivalent residue was discovered as a
322 natural histidine to tyrosine point mutation that decreased function of the *Streptococcus pneumonia*
323 capsule acetylation protein WcjE in clinical isolates (72).

324 A similar role for a conserved intermembrane histidine residue has also been suggested for
325 membrane bound O-acyltransferases containing an MBOAT (IPR004299) rather than AT3 domain
326 (73). These observations support a role of the R/K-X_{10}H motif in coordinating a cytoplasmic derived
327 acetyl-CoA molecule within the membrane bound AT3 domain for transfer of the acetyl group to the
328 SGNH domain, consistent with our model (Fig. 1). AT3 domain-containing proteins are implicated in
329 transferring a wide range of acyl groups such as succinate, isovalerate, and propionate (67, 74, 75);
330 these can all be carried by Coenzyme-A. The proposed mechanism of acetyl donor interaction would
331 provide a potential conserved mechanism for transfer of any of these acyl substituents, supporting
332 the idea that the TMH1 arginine and histidine are fundamentally important for the mechanism of all
333 AT3 domain-containing acyltransferases.

334 Residues specifically conserved in the AT3 domains of AT3-SGNH fused proteins ($OafA_{F35}$ and $OafA_{D39}$
335 in TMH2 and $OafA_{S112}$ between TMH3-4) are located towards the periplasmic side of the AT3 domain
336 (Fig. 2); we suggest these are likely to be important for interaction with the O-antigen substrate or
337 SGNH domain for acetyl group transfer. In contrast to the essential nature of $OafA_{S112}$ in the

338 periplasmic loop between TMH3-4, no functional residues have been identified in the equivalent
339 region of *S. flexneri* Oac (an AT3-only O-antigen acetyltransferase) (57). Conversely, the invariant
340 glycine residue $OafA_{G46}$, which was critical in *S. flexneri* Oac (Oac_{G53}) (*SI Appendix,* Figure S1) (31, 57),
341 could be replaced by alanine without affecting the function of OafA. These observations imply a
342 divergence between AT3-only and AT3-SGNH fused proteins. The location of critical residues specific
343 to the AT3-SGNH fused proteins, further suggest that this divergence occurs at the point of acetyl
344 group transfer to the acceptor substrate.

345 This study demonstrates that the SGNH domain of OafA is able to acetylate the abequose of the O-
346 antigen of *Salmonella in vitro* without the presence of its cognate fused AT3 domain. This supports
347 the predicted role for SGNH in the final step of acetyl group transfer to the acceptor substrate in
348 fused acetyltransferases (Fig. 1*B*). In agreement with this, in the two component PatA/PatB
349 peptidoglycan acetyltransferase system, PatB, a soluble SGNH protein, is responsible for transfer of
350 the acetyl group onto the peptidoglycan substrate (62). Moynihan and Clarke *et al.* hypothesised
351 that PatA (an MBOAT protein not an AT3) is responsible for transporting the acetyl group across the
352 membrane where it is transferred to the acceptor by the soluble PatB protein (62). The membrane
353 bound PatA MBOAT protein in this system is interchangeable with WecH, an AT3-only
354 acetyltransferase protein (52, 76), giving an example of direct transfer of acetate between a
355 membrane bound AT3 domain and soluble SGNH domain protein. This supports the mechanistic
356 model of the AT3 domain delivering the acetyl group to the SGNH domain for transfer onto the
357 acceptor substrate in AT3-SGNH fused proteins (Fig. 1*B*).

358 Our data demonstrated, for the first time in a fused system, the necessity for the fused SGNH
359 domain in glycan carbohydrate acetylation. However, this poses the conundrum that other closely
360 related systems, such as OacA from *Shigella* that O-acetylates rhamnose in the O-antigen (57), lack
361 either a fused or genetically linked partner SGNH domain. Consequently, either the AT3 domain
362 functions differently, or there is a currently undiscovered partner protein.

363 This study elucidates the structure of the $SGNH_{ext}$ in $OafB_{SPA}^{C\text{-}long}$ and shows that removal of this
364 region results in promiscuity of carbohydrate modification in *in vitro* acetyltransferase reactions (Fig.
365 7). These findings suggest that the $SGNH_{ext}$ plays a role in determining the specificity of the O-
366 antigen residue to be acetylated. Closer examination of the structure reveals that two tyrosines,
367 Tyr289 and Tyr394, in the $SGNH_{ext}$ sit closely to the active site and could potentially be involved in a
368 mechanism to limit off-target acetylation. Inadvertent acetylation of complex carbohydrates could
369 potentially have diverse and undesired biological effects due to the variation of cellular processes
370 that can be affected by acetylation (9, 33, 39, 77–79). Whether this also implies that AT3 proteins all
371 need a partner domain or protein for substrate specific transferase activity remains to be
372 determined.

373 Co-evolution analysis predicts interaction between periplasmic loops of the AT3 domain and the
374 SGNH domain of OafB. This is similar to the arrangement of domains seen in PglB, an oligosaccharide
375 transferase from *Campylobacter lari* (80), with 13 TMH and a periplasmic domain. In PglB the
376 periplasmic domain interacts via periplasmic loops in the transmembrane domain and both domains
377 are hypothesised to interact with the peptide substrate (80). In our model, the co-evolution analysis
378 positions the periplasmic loops of the AT3 domain close to α8 helix in the SGNH domain allowing for
379 a interaction with each other and with the acceptor substrate (Fig. 8).

380 AT3 domain-containing proteins are involved in the modification of a wide range of polysaccharides
381 and influence many host-pathogen interactions. These structural and functional insights can be
382 applied to the well-studied and biotechnologically relevant AT3 proteins, including Nod factor
383 modifications important for plant microbe symbiosis, and anti-tumour and antibiotic modifying
384 proteins. Furthermore, this work can inform future studies in eukaryotic systems where AT3 domain-
385 containing proteins are involved in regulation of the lifespan of *Caenorhabditis elegans* (81) and in
386 *Drosophila* development (82).

387

388 # Methods

389 ## Bacterial strains, plasmids and culture conditions:

390 *Escherichia coli* and STM strains and plasmids are listed in *SI Appendix,* Table S2. Strains were
391 cultured in Lennox broth (LB; Fisher Scientific) at 37 °C with appropriate antibiotic selection unless
392 otherwise stated.

393 ## *In silico* analysis of bacterial AT3 domains to identify conserved residues

394 A survey of the literature identified 30 experimentally-characterised bacterial carbohydrate
395 acetyltransferases, these sequences were aligned along with OafB from *Salmonella* ser. Paratyphi A,
396 using TCoffee (83). Protein accession numbers are in Fig. S1. TCoffee was also used to align $OafA_{STM}$,
397 $OafB_{STM}$ and $OafB_{SPA}$ protein sequences for direct comparison.

398 Structure based sequence alignments using PROMALS-3D with default settings were carried out with
399 the two closest structural homologues identified using the DALI server, and a selection of typical
400 SGNH domains for which structural information is available: $OafB_{SPA}$, 1IVN, 4K40, 1DEX, 5UFY, 5B5S
401 and 2VPT. Five further representative sequences of OafA, OafB, and OatA were included
402 (A0A0H2WM30, STMMW_03911, Q8ZNJ3, NTHI0512, Q2FV54).

403 ## Co-evolution analysis

404 A multiple sequence alignment of AT3 SGNH domain fused proteins was constructed using the
405 MUSCLE alignment tool based on 1,188 full length sequences from the UniProt Reference
406 Proteomes. This alignment was used to construct a profile-HMM to detect further homologues in
407 the UniProt Reference Proteome set as well as within the MGnify protein sequence set. We required
408 that all matches to this profile-HMM had a sequence and domain threshold of 27 bits. We also

409 required that the sequence matched > 90% of the HMM match states to ensure that homologues
410 with only one of the two domains were not included in the alignment.

411 2,713 homologues were identified from the UniProt Reference Proteome set and 9,757 homologues
412 were identified from the MGnify metagenomics sequences. A large sequence alignment was
413 constructed using OafB as the master with no indels with all the sequence matches aligned to it
414 using the hmmalign package and a custom Perl script to format the alignment for contact prediction.
415 The alignment was submitted to the RaptorX contact prediction server (84).

416 Molecular Biology

417 Primers (Sigma-Aldrich) are listed in *SI Appendix,* Table S2. Mutations were introduced into the OafA
418 sequence (pMV433 as template), which had been cloned into pBADcLIC using blunt end ligation,
419 placing the gene under control of an arabinose inducible promoter. Mutants were confirmed by
420 sequencing. Plasmids were electroporated into STM strain 293 (*SI Appendix,* Table S2) for analysis of
421 activity.

422 All $oafA_{STM}$ and $oafB_{SPA}$ sequences for protein expression were cloned into pETFPP_2 (Technology
423 Facility, University of York) using in-fusion cloning (Clontech) to add a 3C-protease cleavable N-
424 terminal His-MBP tag. Plasmid pMV433 (*SI Appendix,* Table S2) was used as the template for creation
425 of expression plasmids encoding the protein sequence for $OafA_{STM}^{C\text{-}long}$ (residues 366-609) and
426 $OafA_{STM}^{C\text{-}short}$ (residues 379-609). $oafB_{SPA}$ (A0A0H2WM30) amino acid residues 377 to 640 for
427 $OafB_{SPA}^{C\text{-}long}$, was codon-optimised for *E. coli* and synthesised by Genewiz in a pUC57-Kan vector. This
428 vector was then used as a template for the sequence encoding $OafB_{SPA}^{C\text{-}short}$ (residues 399-640); see
429 *SI Appendix,* Table S2 for primers used.

430 *In situ* functional analysis of OafA variants

431 All *in situ* functional analyses of OafA variants cloned into pBADcLIC were carried out in strain
432 Path293 (23) (*SI Appendix,* Table S2). Strains for the *in situ* functional analysis were cultured at pH
433 7.0 in 100 mM sodium phosphate-buffered LB at 37 °C in a baffled conical flask with shaking at 200
434 rpm. Overnight cultures were diluted 100-fold and grown for 16 hr. Samples were normalised to
435 (OD_{600}) of 3.0 per ml for LPS and protein extraction.

436 Crude LPS sample preparation

437 The method was adapted from Davies *et al.* 2013 (23). 1 ml of OD-normalised (OD_{600} 3.0) overnight
438 culture was pelleted for 5 min at 16,000xg. Cell pellets were re-suspended in 100 µl LPS sample
439 buffer (60 mM Tris-HCL, 1mM EDTA, pH 6.8) containing 2% (w/v) SDS then boiled at 100 °C for 5 min.
440 400 µl of LPS buffer was then used to dilute the solution before RNAse (Roche) and DNAse (Sigma)
441 treatment at 37 ˚C for 16 hours. Samples were then treated with 100 µg proteinase K for 16 hours at
442 50 ˚C. 7.5 µl of crude LPS extracts were run on 1.0 mm Tricine SDS - Poly Acrylamide Gel
443 Electrophoresis TSDS-PAGE gel for analysis by immunoblotting.

444 Detection of OafA protein expression for *in situ* assays

445 1ml of OD-normalised culture was pelleted for 5 min at 16,000xg. Soluble and insoluble fractions
446 were isolated from cell pellets using Bug Buster™ solution (Novagen) following manufacturer's
447 instructions for soluble protein extraction. The insoluble pellet was resuspended in 75 µl of sample
448 buffer (10% (v/v) Glycerol, 1% (w/v) SDS, 10mM Tris-HCL, pH 7.2, 0.06% (w/v) Bromophenol Blue, 3%
449 (v/v) β-mercaptoethanol), heated to 60˚C for 10 min and centrifuged for 10 min at 16,000xg. 10 µl of
450 insoluble fraction samples were loaded onto a 12% acrylamide 1.0 mm SDS-PAGE gel for analysis.

451 Immunoblotting

452 7.5 µl of crude LPS extracts were run on 1.0 mm Tricine SDS - Polyacrylamide Gel Electrophoresis
453 (TSDS-PAGE) gel for analysis by immunoblotting. The TSDS-PAGE-separated LPS samples and SDS-

454 PAGE separated protein samples were transferred onto Immobilon-P PVDF membrane (Merck-
455 Millipore). For His-tagged protein detection, the primary antibody was Tetra·His Antibody (1:1000)
456 (Qiagen; in 3% (w/v) BSA TBS) and the secondary antibody was goat anti-mouse IgG-HRP (1:10000)
457 (Sigma-Aldrich; in 5% (w/v) Milk TBS). The blot was developed using Luminata Classico Western HRP
458 substrate (Merck-Millipore). For LPS detection O:5 serotyping antibody (1:10000) (Statens Serum
459 Institute; 40272) and *Salmonella* core antigen (1:200) (Insight Biotechnology; 5D12A) were used as
460 the primary antibodies and Goat Anti-Rabbit IgG StarBright Blue700 (1:5000) (Bio-Rad) and Goat
461 anti-mouse IgG (H+L) DyLight 800 (1:5000) as the respective secondary antibodies. LPS antibodies
462 were diluted in 5% Milk PBS-T. ChemiDoc MP Imaging System (Bio-Rad) and Image Lab™ (Bio-Rad)
463 were used for image capture and analysis. The *in situ* activity of OafA mutant relative to wild type
464 protein was derived from quantification of the O:5 signal in each lane, standardised to the intensity
465 of the single O-antigen repeat band for the *Salmonella* core signal on LPS immunoblots. Assay
466 validation demonstrated that <1% O:5 signal with respect to wild type was within the background
467 variation. Variation increased significantly for signal intensities in the higher range, therefore O:5
468 signal recoded between 50 and 100% relative to wild type was not interpreted further.

469 **Expression and purification of $OafA_{STM}^{C\text{-}term}$ and $OafB_{SPA}^{C\text{-}term}$**

470 pETFPP_2 vectors containing the inserted $OafA_{STM}^{C\text{-}term}$ and $OafB_{SPA}^{C\text{-}term}$ constructs (Fig. 1) were
471 transformed into Origami (Novagen) *E. coli* for protein expression. Protein expression was carried
472 out as described by Gruszka et al. 2015 (85) without the addition of protease inhibitor. The proteins
473 were purified using immobilised metal affinity chromatography with a HisTrap FF column (GE
474 Healthcare) utilising a His-tag, followed by size exclusion chromatography after His-tag removal, as
475 described by Gruszka et al. 2012 (86); purified protein was eluted in 20 mM Tris-HCl pH 7.5, 100 mM
476 NaCl.

477 **Melting temperature of OafA and OafB SGNH domains**

478 The melting temperature of SGNH domains was determined using NanoDSF with a protein
479 concentration of 1 mg/mL in 20 mM TrisHCl pH 7.5, 100 mM NaCl. Proteins were heated from 20 ^{o}C
480 to 95 ^{o}C with a heating rate of 2 ^{o}C / min. The fluorescence at 330 and 350 nm was measured every
481 0.05 ^{o}C.

482 ***In vitro* acetylesterase activity assay**

483 The catalytic activity of OafA and OafB C-terminal constructs was confirmed by acetyl esterase
484 activity using pNP-Ac as a substrate. 100 µl of enzyme solution (10 µM $OafA_{STM}^{C\text{-}term}$, 40 µM $OafB_{STM}^{C\text{-}}$
485 ^{term} or 0.04 U/ml Acetylxylanesterase) or appropriate control buffers were added to relevant wells of
486 a 96 well plate and incubated at 37 ˚C for 10 min prior to addition of pNP-Ac. 100 µl of 1 mM pNPA
487 in the corresponding buffer was then added to matching sample and control wells and immediately
488 placed into a plate reader incubated at 37 ˚C. Absorbance at 405 nm was measured at T=0, and then
489 at 5 min intervals.

490 ***In vitro* abequose acetyltransferase activity assay**

491 Crude LPS extracted from OafA-negative STM LT2 strain (Path993) was heated at 100°C for 20 min to
492 inactivate the proteinase K (see above). Heat-treated LPS was mixed 1:1 with KPi buffer (200 mM
493 NaCl, 50 mM Potassium Phosphate buffer pH 7.8). 10 µM $OafA_{STM}^{C\text{-}term}$ and 20 µM $OafB_{SPA}^{C\text{-}term}$ were
494 incubated at 4 °C in LPS-KPi mixture with 4 mM pNP-Ac dissolved in ethanol (4% (v/v) final
495 concentration in reaction). Samples of the reaction mix were taken after specified time points and
496 inactivated by boiling for 10 min.

497 5 µl of LPS reaction samples were loaded onto methanol-activated PVDF membrane using a BioRad
498 Bio-Dot® microfiltration apparatus. The protocol for LPS detection with O:5 serotyping antibodies

499 and *Salmonella* core antigen was followed as per immunoblotting, following removal of the
500 membrane from the apparatus after sample loading.

501 Protein structure analysis

502 To crystallise $OafB_{SPA}^{C\text{-}long}$, a hanging-drop vapour diffusion method was used with 20 mg/mL
503 $OafB_{SPA}^{C\text{-}long}$ in a drop ratio of 1:1 protein:reservoir solution. After incubation for 24 hours at 20°C
504 crystals grown in 100 mM BisTris pH 5.5, 0.25 M lithium sulfate, 25% PEG 3350 were cryoprotected
505 by addition of glycerol to a final concentration of 20% and vitrified in liquid nitrogen.

506 X-ray diffraction data for crystals of $OafB_{SPA}^{C\text{-}long}$ were collected on beamline I04-1 (Diamond Light
507 Source, UK) at a wavelength of 0.9282 Å using a Pilatus 6M-F detector. Data were integrated with
508 XDS (87), and scaled and merged with AIMLESS (88) via the Xia2 pipeline (89). Fragon molecular
509 replacement (59) used Phaser (90) to place an ideal poly-alanine helix of 14 amino acids in length
510 followed by density modification with ACORN (91). ARP-wARP (92) was used for automated chain
511 tracing, and the model was refined using REFMAC5 (93–98). Manual manipulation of the model
512 between refinement cycles was performed using Coot (99, 100). The final model was evaluated using
513 MolProbity (101) and PDB validate, secondary structure shown in Fig. 5A was annotated using
514 STRIDE (102).

515 A homology model of $OafA_{STM}^{C\text{-}long}$ was produced using SwissModel with the structure of $OafB_{SPA}^{C\text{-}long}$
516 as a template (103–107).

517 **Data Availability**

518 The atomic coordinates and structure factors have been deposited in the Protein Data Bank (PDB ID
519 code 6SE1).

520 # Acknowledgments

521 CP and ST were supported by a PhD studentship from the Biotechnology and Biological Sciences
522 Research Council White Rose Doctoral Training Programme (BB/M011151/1): Mechanistic Biology
523 and its Strategic Application. The authors thank the support of the University of York Technology
524 Facility, Steinar Mannsverk for technical assistance and Jean Whittingham for crystallography
525 support. The authors thank Diamond Light Source for access to beamline I04-1 (under proposal DLS-
526 MX-13587).

527 # References

528 1. Majowicz SE, Musto J, Scallan E, Angulo FJ, Kirk M, O'Brien SJ, Jones TF, Fazil A, Hoekstra RM.
529 2010. The Global Burden of Nontyphoidal Salmonella Gastroenteritis. Clin Infect Dis 50:882–
530 889.

531 2. Hiyoshi H, Tiffany CR, Bronner DN, Bäumler AJ. 2018. Typhoidal Salmonella serovars:
532 ecological opportunity and the evolution of a new pathovar. FEMS Microbiol Rev. 42:527-541.

533 3. Reddy EA, Shaw A V, Crump JA. 2010. Community-acquired bloodstream infections in Africa:
534 a systematic review and meta-analysis. Lancet Infect Dis 10:417–32.

535 4. Crump JA, Luby SP, Mintz ED. 2004. The global burden of typhoid fever. Bull World Health
536 Organ 82:346–353.

537 5. Lynch MF, Blanton EM, Bulens S, Polyak C, Vojdani J, Stevenson J, Medalla F, Barzilay E, Joyce
538 K, Barrett T, Mintz ED. 2009. Typhoid Fever in the United States, 1999-2006. JAMA 302:859.

539 6. Boore AL, Hoekstra RM, Iwamoto M, Fields PI, Bishop RD, Swerdlow DL. 2015. Salmonella
540 enterica Infections in the United States and Assessment of Coefficients of Variation: A Novel
541 Approach to Identify Epidemiologic Characteristics of Individual Serotypes, 1996-2011. PLoS
542 One 10:e0145416.

543 7. Liu B, Knirel YA, Feng L, Perepelov A V., Senchenkova SN, Reeves PR, Wang L. 2014. Structural
544 diversity in Salmonella O antigens and its genetic basis. FEMS Microbiol Rev 38:56–89.

545 8. Raetz C, Whitfield C. 2002. Lipopolysaccharide endotoxins. Annu Rev Biochem 71:635–700.

546 9. Kintz E, Davies MR, Hammarlöf DL, Canals R, Hinton JCDD, van der Woude MW. 2015. A BTP1
547 prophage gene present in invasive non-typhoidal S almonella determines composition and
548 length of the O-antigen of the lipopolysaccharide. Mol Microbiol 96:263–275.

549 10. Kintz E, Heiss C, Black I, Donohue N, Brown N, Davies MR, Azadi P, Baker S, Kaye PM, van der
550 Woude M. 2017. Salmonella Typhi Lipopolysaccharide O-antigen Modifications Impact on
551 Serum Resistance and Antibody Recognition. Infect Immun 85:e01021-16.

552 11. Kim ML, Slauch JM. 1999. Effect of acetylation (O-factor 5) on the polyclonal antibody
553 response to Salmonella typhimurium O-antigen. FEMS Immunol Med Microbiol 26:83–92.

554 12. Fierer J, Guiney DG. 2001. Diverse virulence traits underlying different clinical outcomes of

555 Salmonella infection. J Clin Invest 107:775–80.

556 13. Moynihan PJ, Clarke AJ. 2011. O-Acetylated peptidoglycan: Controlling the activity of
557 bacterial autolysins and lytic enzymes of innate immune systems. Int J Biochem Cell Biol
558 43:1655–1659.

559 14. Bera A, Herbert S, Jakob A, Vollmer W, Götz F. 2005. Why are pathogenic staphylococci so
560 lysozyme resistant? The peptidoglycan O-acetyltransferase OatA is the major determinant for
561 lysozyme resistance of Staphylococcus aureus. Mol Microbiol 55:778–787.

562 15. Davis EO, Evans IJ, Johnston AWB. 1988. Identification of nodX, a gene that allows Rhizobium
563 leguminosarum biovar viciae strain TOM to nodulate Afghanistan peas. MGG Mol Gen Genet
564 212:531–535.

565 16. Verma NK, Brandt JM, Verma DJ, Lindberg AA. 1991. Molecular characterization of the O-
566 acetyl transferase gene of converting bacteriophage SF6 that adds group antigen 6 to Shigella
567 flexneri. Mol Microbiol 5:71–75.

568 17. Slauch JM, Lee AA, Mahan MJ, Mekalanos JJ. 1996. Molecular characterization of the oafA
569 locus responsible for acetylation of Salmonella typhimurium O-antigen: OafA is a member of
570 a family of integral membrane trans-acylases. J Bacteriol 178:5904–5909.

571 18. Clark CA, Beltrame J, Manning PA. 1991. The oac gene encoding a lipopolysaccharide O-
572 antigen acetylase maps adjacent to the integrase-encoding gene on the genome of Shigella
573 flexneri bacteriophage Sf6. Gene 107:43–52.

574 19. Dalrymple BP, Cybinski DH, Layton I, McSweeney CS, Xue GP, Swadling YJ, Lowry JB. 1997.
575 Three Neocallimastix patriciarum esterases associated with the degradation of complex
576 polysaccharides are members of a new family of hydrolases. Microbiology 143:2605–2614.

577 20. Mølgaard A, Kauppinen S, Larsen S. 2000. Rhamnogalacturonan acetylesterase elucidates the
578 structure and function of a new family of hydrolases. Structure 8:373–383.

579 21. Lombard V, Golaconda Ramulu H, Drula E, Coutinho PM, Henrissat B. 2014. The
580 carbohydrate-active enzymes database (CAZy) in 2013. Nucleic Acids Res 42:D490-495.

581 22. Akoh CC, Lee G-C, Liaw Y-C, Huang T-H, Shaw J-F. 2004. GDSL family of serine
582 esterases/lipases. Prog Lipid Res 43:534–52.

583 23. Davies MR, Broadbent SE, Harris SR, Thomson NR, van der Woude MW. 2013. Horizontally

584 Acquired Glycosyltransferase Operons Drive Salmonellae Lipopolysaccharide Diversity. PLoS
585 Genet 9:e1003568.

586 24. Slauch JM, Mahan MJ, Michetti P, Neutra MR, Mekalanos JJ. 1995. Acetylation (O-factor 5)
587 affects the structural and immunological properties of Salmonella typhimurium
588 lipopolysaccharide O antigen. Infect Immun 63:437–41.

589 25. Grimont P, Weill F-X. 2008. Antigenic formulae of the Salmonella servovars. WHO Collab
590 Cent Ref Res Salmonella 1–167.

591 26. Issenhuth-Jeanjean S, Roggentin P, Mikoleit M, Guibourdenche M, de Pinna E, Nair S, Fields
592 PI, Weill FX. 2014. Supplement 2008-2010 (no. 48) to the White-Kauffmann-Le Minor scheme.
593 Res Microbiol 165:526–530.

594 27. Lanzilao L, Stefanetti G, Saul A, MacLennan CA, Micoli F, Rondini S. 2015. Strain selection for
595 generation of O-antigen-based glycoconjugate vaccines against invasive nontyphoidal
596 Salmonella disease. PLoS One 10:e0139847.

597 28. Mitchell A, Chang H-Y, Daugherty L, Fraser M, Hunter S, Lopez R, McAnulla C, McMenamin C,
598 Nuka G, Pesseat S, Sangrador-Vegas A, Scheremetjew M, Rato C, Yong S-Y, Bateman A, Punta
599 M, Attwood TK, Sigrist CJA, Redaschi N, Rivoire C, Xenarios I, Kahn D, Guyot D, Bork P, Letunic
600 I, Gough J, Oates M, Haft D, Huang H, Natale DA, Wu CH, Orengo C, Sillitoe I, Mi H, Thomas
601 PD, Finn RD. 2015. The InterPro protein families database: the classification resource after 15
602 years. Nucleic Acids Res 43:D213-21.

603 29. Finn RD, Bateman A, Clements J, Coggill P, Eberhardt RY, Eddy SR, Heger A, Hetherington K,
604 Holm L, Mistry J, Sonnhammer ELL, Tate J, Punta M. 2014. Pfam: the protein families
605 database. Nucleic Acids Res 42:D222-30.

606 30. Krogh A, Larsson B, Von Heijne G, Sonnhammer EL. 2001. Predicting transmembrane protein
607 topology with a hidden Markov model: Application to complete genomes. J Mol Biol
608 305:567–580.

609 31. Thanweer F, Verma NK. 2012. Identification of critical residues of the serotype modifying O-
610 acetyltransferase of Shigella flexneri. BMC Biochem 13:13.

611 32. Crisóstomo MI, Vollmer W, Kharat AS, Inhülsen S, Gehre F, Buckenmaier S, Tomasz A. 2006.
612 Attenuation of penicillin resistance in a peptidoglycan O-acetyl transferase mutant of
613 Streptococcus pneumoniae. Mol Microbiol 61:1497–1509.

614 33. Laaberki MH, Pfeffer J, Clarke AJ, Dworkin J. 2011. O-acetylation of peptidoglycan is required
615 for proper cell separation and S-layer anchoring in Bacillus anthracis. J Biol Chem 286:5278–
616 5288.

617 34. Buendia AM, Enenkel B, Köplin R, Niehaus K, Arnold W, Pünier A. 1991. The Rhizobium
618 meliloti exoZl exoB fragment of megaplasmid 2: ExoB functions as a UDP-glucose 4-epimerase
619 and ExoZ shows homology to NodX of Rhizobium leguminosarum biovar viciae strain TOM.
620 Mol Microbiol. 5:1519-1530.

621 35. Katzen F, Ferreiro DU, Oddo CG, Ielmini M V, Becker A, Pühler A, Ielpi L. 1998. Xanthomonas
622 campestris pv. campestris gum mutants: effects on xanthan biosynthesis and plant virulence.
623 J Bacteriol 180:1607–17.

624 36. Fox KL, Yildirim HH, Deadman ME, Schweda EKH, Moxon ER, Hood DW. 2005. Novel
625 lipopolysaccharide biosynthetic genes containing tetranucleotide repeats in Haemophilus
626 influenzae, identification of a gene for adding O-acetyl groups. Mol Microbiol 58:207–216.

627 37. Zou CH, Knirel YA, Helbig JH, Zähringer U, Mintz CS. 1999. Molecular cloning and
628 characterization of a locus responsible for O acetylation of the O polysaccharide of Legionella
629 pneumophila serogroup 1 lipopolysaccharide. J Bacteriol 181:4137–41.

630 38. Aubry C, Goulard C, Nahori MA, Cayet N, Decalf J, Sachse M, Boneca IG, Cossart P, Dussurget
631 O. 2011. OatA, a peptidoglycan O-acetyltransferase involved in Listeria monocytogenes
632 immune escape, is critical for virulence. J Infect Dis 204:731–740.

633 39. Kahler CM, Lyons-Schindler S, Choudhury B, Glushka J, Carlson RW, Stephens DS. 2006. O-
634 acetylation of the terminal N-acetylglucosamine of the lipooligosaccharide inner core in
635 Neisseria meningitidis: Influence on inner core structure and assembly. J Biol Chem
636 281:19939–19948.

637 40. Bernard E, Rolain T, Courtin P, Guillot A, Langella P, Hols P, Chapot-Chartier M-P. 2011.
638 Characterization of *O* -Acetylation of *N* -Acetylglucosamine. J Biol Chem 286:23950–23958.

639 41. Pacios Bras C, Jordá MA, Wijfjes a H, Harteveld M, Stuurman N, Thomas-Oates JE, Spaink HP.
640 2000. A Lotus japonicus nodulation system based on heterologous expression of the fucosyl
641 transferase NodZ and the acetyl transferase NoIL in Rhizobium leguminosarum. Mol Plant
642 Microbe Interact 13:475–479.

643 42. Brett PJ, Burtnick MN, Heiss C, Azadi P, DeShazer D, Woods DE, Gherardini FC. 2011.

644 Burkholderia thailandensis oacA mutants facilitate the expression of Burkholderia mallei-like
645 O polysaccharides. Infect Immun 79:961–9.

646 43. Wang J, Knirel YA, Lan R, Senchenkova SN, Luo X, Perepelov A V, Wang Y, Shashkov AS, Xu J,
647 Sun Q. 2014. Identification of an O-acyltransferase gene (oacB) that mediates 3- and 4-O-
648 acetylation of rhamnose III in Shigella flexneri O antigens. J Bacteriol 196:1525–31.

649 44. Knirel YA, Wang J, Luo X, Senchenkova SN, Lan R, Shpirt AM, Du P, Shashkov AS, Zhang N, Xu
650 J, Sun Q. 2014. Genetic and structural identification of an O-acyltransferase gene (oacC)
651 responsible for the 3/4-O-acetylation on rhamnose III in Shigella flexneri serotype 6. BMC
652 Microbiol 14:266.

653 45. Sun Q, Knirel YA, Wang J, Luo X, Senchenkova SN, Lan R, Shashkov AS, Xu J. 2014. Serotype-
654 converting bacteriophage SfII encodes an acyltransferase protein that mediates 6-O-
655 acetylation of GlcNAc in Shigella flexneri O-antigens, conferring on the host a novel O-antigen
656 epitope. J Bacteriol 196:3656–3666.

657 46. Cogez V, Gak E, Puskas A, Kaplan S, Bohin JP. 2002. The opgGIH and opgC genes of
658 Rhodobacter sphaeroides form an operon that controls backbone synthesis and succinylation
659 of osmoregulated periplasmic glucans. Eur J Biochem 269:2473–2484.

660 47. Bontemps-Gallo S, Madec E, Robbe-Masselot C, Souche E, Dondeyne J, Lacroix J-M. 2016. The
661 opgC gene is required for OPGs succinylation and is osmoregulated through RcsCDB and
662 EnvZ/OmpR in the phytopathogen Dickeya dadantii. Sci Rep 6:19619.

663 48. Hong Y, Duda KA, Cunneen MM, Holst O, Reeves PR. 2013. The WbaK acetyltransferase of
664 Salmonella enterica group E gives insights into O antigen evolution. Microbiol (United
665 Kingdom) 159:2316–2322.

666 49. Brett PJ, Burtnick M, Woods D. 2003. The wbiA locus is required for the 2-O-acetylation of
667 lipopolysaccharides expressed by Burkholderia pseudomallei and Burkholderia thailandensis.
668 FEMS Microbiol Lett. 218:323-328.

669 50. Geno KA, Saad JS, Nahm MH. 2017. Discovery of novel pneumococcal serotype 35D, a natural
670 WciG-deficient variant of serotype 35B. J Clin Microbiol 55:1416–1425.

671 51. Calix JJ, Nahm MH. 2010. A new pneumococcal serotype, 11E, has a variably inactivated wcjE
672 gene. J Infect Dis 202:29–38.

673 52. Kajimura J, Rahman A, Hsu J, Evans MR, Gardner KH, Rick PD. 2006. O Acetylation of the

674 Enterobacterial Common Antigen Polysaccharide Is Catalyzed by the Product of the yiaH
675 Gene of Escherichia coli K-12. J Bacteriol 188:7542–7550.

676 53. Veiga P, Bulbarela-Sampieri C, Furlan S, Maisons A, Chapot-Chartier M-P, Erkelenz M,
677 Mervelet P, Noirot P, Frees D, Kuipers OP, Kok J, Gruss A, Buist G, Kulakauskas S. 2007. SpxB
678 Regulates O-Acetylation-dependent Resistance of Lactococcus lactis Peptidoglycan to
679 Hydrolysis. J Biol Chem 282:19342–19354.

680 54. Menéndez N, Nur-e-Alam M, Braña AF, Rohr J, Salas JA, Méndez C. 2004. Biosynthesis of the
681 Antitumor Chromomycin A3 in Streptomyces griseus: Analysis of the Gene Cluster and
682 Rational Design of Novel Chromomycin Analogs. Chem Biol 11:21–32.

683 55. Warren MJ, Roddam LF, Power PM, Terry TD, Jennings MP. 2004. Analysis of the role of pglI
684 in pilin glycosylation of Neisseria meningitidis. FEMS Immunol Med Microbiol 41:43–50.

685 56. Hauser E, Junker E, Helmuth R, Malorny B. 2011. Different mutations in the oafA gene lead to
686 loss of O5-antigen expression in Salmonella enterica serovar Typhimurium. J Appl Microbiol
687 110:248–253.

688 57. Thanweer F, Tahiliani V, Korres H, Verma NK. 2008. Topology and identification of critical
689 residues of the O-acetyltransferase of serotype-converting bacteriophage, SF6, of Shigella
690 flexneri. Biochem Biophys Res Commun 375:581–585.

691 58. Ravenscroft N, Cescutti P, Gavini M, Stefanetti G, Maclennan CA, Martin LB, Micoli F. 2015.
692 Structural analysis of the O-acetylated O-polysaccharide isolated from Salmonella paratyphi A
693 and used for vaccine preparation. Carbohydr Res 404:108–116.

694 59. Jenkins HT. 2018. Fragon: rapid high-resolution structure determination from ideal protein
695 fragments. Acta Crystallogr Sect D Struct Biol 74:205–214.

696 60. Sychantha D, Jones CS, Little DJ, Moynihan PJ, Robinson H, Galley NF, Roper DI, Dowson CG,
697 Howell PL, Clarke AJ. 2017. In vitro characterization of the antivirulence target of Gram-
698 positive pathogens, peptidoglycan O-acetyltransferase A (OatA). PLoS Pathog 13:e1006667.

699 61. Lee L-C, Lee Y-L, Leu R-J, Shaw J-F. 2006. Functional role of catalytic triad and oxyanion hole-
700 forming residues on enzyme activity of Escherichia coli thioesterase I/protease
701 I/phospholipase L1. Biochem J 397:69–76.

702 62. Moynihan PJ, Clarke AJ. 2014. Substrate specificity and kinetic characterization of
703 peptidoglycan O-acetyltransferase B from Neisseria gonorrhoeae. J Biol Chem 289:16748–

704 16760.

705 63. Pfeffer JM, Weadge JT, Clarke AJ. 2013. Mechanism of action of neisseria gonorrhoeae O-
706 acetylpeptidoglycan esterase, an SGNH serine esterase. J Biol Chem 288:2605–2613.

707 64. Baker P, Ricer T, Moynihan PJ, Kitova EN, Walvoort MTC, Little DJ, Whitney JC, Dawson K,
708 Weadge JT, Robinson H, Ohman DE, Codée JDC, Klassen JS, Clarke AJ, Howell PL. 2014. P.
709 aeruginosa SGNH Hydrolase-Like Proteins AlgJ and AlgX Have Similar Topology but Separate
710 and Distinct Roles in Alginate Acetylation. PLoS Pathog 10: e1004334.

711 65. Moynihan PJ, Clarke AJ. 2013. Assay for peptidoglycan O-acetyltransferase: A potential new
712 antibacterial target. Anal Biochem 439:73–79.

713 66. Menéndez N, Nur-e-Alam M, Braña AF, Rohr J, Salas JA, Méndez C. 2004. Tailoring
714 modification of deoxysugars during biosynthesis of the antitumour drug chromomycin A3 by
715 Streptomyces griseus ssp. griseus. Mol Microbiol 53:903–915.

716 67. Arisawa A, Kawamura N, Tsunekawa H, Okamura K, Tone H, Okamoto R. 1993. Cloning and
717 nucleotide sequences of two genes involved in the 4''-O-acylation of macrolide antibiotics
718 from Streptomyces thermotolerans. Biosci Biotechnol Biochem 57:2020–5.

719 68. Takamura Y NG. 1988. Changes in the intracellular concentration of acetyl-CoA and malonyl-
720 CoA in relation to the carbon and energy metabolism of Escherichia coli K12. J Gen Microbiol
721 134:224:2249–2253.

722 69. Krivoruchko A, Zhang Y, Siewers V, Chen Y, Nielsen J. 2015. Microbial acetyl-CoA metabolism
723 and metabolic engineering. Metab Eng 28:28–42.

724 70. Wu D, Hersh LB. 1995. Identification of an active site arginine in rat choline acetyltransferase
725 by alanine scanning mutagenesis. J Biol Chem 270:29111–6.

726 71. JOGL G, HSIAO Y-S, TONG L. 2004. Structure and Function of Carnitine Acyltransferases. Ann
727 N Y Acad Sci 1033:17–29.

728 72. Calix JJ, Oliver MB, Sherwood LK, Beall BW, Hollingshead SK, Nahm MH. 2011. Streptococcus
729 pneumoniae Serotype 9A Isolates Contain Diverse Mutations to wcjE That Result in Variable
730 Expression of Serotype 9V-specific Epitope. J Infect Dis 204:1585–1595.

731 73. Ma D, Wang Z, Merrikh CN, Lang KS, Lu P, Li X, Merrikh H, Rao Z, Xu W. 2018. Crystal structure
732 of a membrane-bound O-acyltransferase. Nature 562:286-290.

733 74. Roset MS, Ciocchini AE, Ugalde RA, Inon de Iannino N. 2006. The Brucella abortus Cyclic -1,2-
734 Glucan Virulence Factor Is Substituted with O-Ester-Linked Succinyl Residues. J Bacteriol
735 188:5003–5013.

736 75. Cong L, Piepersberg W. 2007. Cloning and characterization of genes encoded in dTDP-D-
737 mycaminose biosynthetic pathway from a midecamycin-producing strain, streptomyces
738 mycarofaciens. Acta Biochim Biophys Sin (Shanghai) 39:187–193.

739 76. Moynihan PJ, Clarke AJ. 2010. O-acetylation of peptidoglycan in gram-negative bacteria:
740 Identification and characterization of peptidoglycan O-acetyltransferase in Neisseria
741 gonorrhoeae. J Biol Chem 285:13264–13273.

742 77. Bernard E, Rolain T, David B, André G, Dupres V, Dufrêne YF, Hallet B, Chapot-Chartier M-PP,
743 Hols P. 2012. Dual Role for the O-Acetyltransferase OatA in Peptidoglycan Modification and
744 Control of Cell Septation in Lactobacillus plantarum PLoS One 7:e47893.

745 78. Baranwal G, Mohammad M, Jarneborn A, Reddy BR, Golla A, Chakravarty S, Biswas L, Götz F,
746 Shankarappa S, Jin T, Biswas R. 2017. Impact of cell wall peptidoglycan O-acetylation on the
747 pathogenesis of Staphylococcus aureus in septic arthritis. Int J Med Microbiol 307:388–397.

748 79. Knirel YA, Prokhorov NS, Shashkov AS, Ovchinnikova OG, Zdorovenko EL, Liu B, Kostryukova
749 ES, Larin AK, Golomidova AK, Letarov A V. 2015. Variations in O-antigen biosynthesis and O-
750 acetylation associated with altered phage sensitivity in Escherichia coli 4s. J Bacteriol
751 197:905–912.

752 80. Lizak C, Gerber S, Numao S, Aebi M, Locher KP. 2011. X-ray structure of a bacterial
753 oligosaccharyltransferase. Nature 474: 350-355.

754 81. Vora M, Shah M, Ostafi S, Onken B, Xue J, Ni JZ, Gu S, Driscoll M. 2013. Deletion of microRNA-
755 80 Activates Dietary Restriction to Extend C. elegans Healthspan and Lifespan. PLoS Genet
756 9:e1003737.

757 82. Dzitoyeva S, Dimitrijevic N, Manev H. 2003. Identification of a novel Drosophila gene, beltless
758 , using injectable embryonic and adult RNA interference (RNAi). BMC Genomics 4:33.

759 83. Notredame C, Higgins DG, Heringa J. 2000. T-coffee: A novel method for fast and accurate
760 multiple sequence alignment. J Mol Biol 302:205–217.

761 84. Källberg M, Margaryan G, Wang S, Ma J, Xu J. 2014. Raptorx server: A resource for template-
762 based protein structure modeling. Methods Mol Biol 1137:17–27.

763 85. Gruszka DT, Whelan F, Farrance OE, Fung HKH, Paci E, Jeffries CM, Svergun DI, Baldock C,
764 Baumann CG, Brockwell DJ, Potts JR, Clarke J. 2015. Cooperative folding of intrinsically
765 disordered domains drives assembly of a strong elongated protein. Nat Commun 6:7271.

766 86. Wojdyla JA, Gruszka DT, Foster TJ, Geoghegan JA, Manfield IW, Bingham RJ, Potts JR,
767 Turkenburg JP, Leech AP, Clarke J, Steward A. 2012. Staphylococcal biofilm-forming protein
768 has a contiguous rod-like structure. Proc Natl Acad Sci 109:E1011–E1018.

769 87. Kabsch W, IUCr. 2010. *XDS*. Acta Crystallogr Sect D Biol Crystallogr 66:125–132.

770 88. Evans PR, Murshudov GN. 2013. How good are my data and what is the resolution? Acta
771 Crystallogr D Biol Crystallogr 69:1204–14.

772 89. Winter G. 2010. xia2: an expert system for macromolecular crystallography data reduction. J
773 Appl Cryst 43:186–190.

774 90. McCoy AJ, Grosse-Kunstleve RW, Adams PD, Winn MD, Storoni LC, Read RJ, IUCr. 2007.
775 *Phaser* crystallographic software. J Appl Crystallogr 40:658–674.

776 91. Jia-Xing Y, Woolfson MM, Wilson KS, Dodson EJ. 2005. A modified ACORN to solve protein
777 structures at resolutions of 1.7 A or better. Acta Crystallogr Sect D Biol Crystallogr 61:1465–
778 1475.

779 92. Perrakis A, Morris R, Lamzin VS. 1999. Automated protein model building combined with
780 iterative structure refinement. Nat Struct Biol 6:458–463.

781 93. Murshudov GN, Skubák P, Lebedev AA, Pannu NS, Steiner RA, Nicholls RA, Winn MD, Long F,
782 Vagin AA, IUCr. 2011. *REFMAC* 5 for the refinement of macromolecular crystal structures.
783 Acta Crystallogr Sect D Biol Crystallogr 67:355–367.

784 94. Vagin AA, Steiner RA, Lebedev AA, Potterton L, McNicholas S, Long F, Murshudov GN. 2004.
785 *REFMAC* 5 dictionary: organization of prior chemical knowledge and guidelines for its use.
786 Acta Crystallogr Sect D Biol Crystallogr 60:2184–2195.

787 95. Nicholls RA, Long F, Murshudov GN, IUCr. 2012. Low-resolution refinement tools in *REFMAC*
788 5. Acta Crystallogr Sect D Biol Crystallogr 68:404–417.

789 96. Murshudov GN, Vagin AA, Lebedev A, Wilson KS, Dodson EJ. 1999. Efficient anisotropic
790 refinement of macromolecular structures using FFT. Acta Crystallogr Sect D Biol Crystallogr
791 55:247–255.

792 97. Winn MD, Murshudov GN, Papiz MZ. 2003. Macromolecular TLS Refinement in REFMAC at
793 Moderate Resolutions, p. 300–321. *In* .

794 98. Garib N. Murshudov; Alexei A. Vagin; Eleanor J. Dodson. 1997. Refinement of
795 Macromolecular Structures by the Maximum-Likelihood Method. Acta Crystallogr Sect D Biol
796 Crystallogr D53:240–255.

797 99. Emsley P, Cowtan K, IUCr. 2004. *Coot* : model-building tools for molecular graphics. Acta
798 Crystallogr Sect D Biol Crystallogr 60:2126–2132.

799 100. Emsley P, Lohkamp B, Scott WG, Cowtan K. 2010. Features and development of Coot. Acta
800 Crystallogr Sect D Biol Crystallogr 66:486–501.

801 101. Chen VB, Arendall WB, Headd JJ, Keedy DA, Immormino RM, Kapral GJ, Murray LW,
802 Richardson JS, Richardson DC, Richardson DC. 2010. MolProbity: all-atom structure validation
803 for macromolecular crystallography. Acta Crystallogr D Biol Crystallogr 66:12–21.

804 102. Heinig M, Frishman D. 2004. STRIDE: a web server for secondary structure assignment from
805 known atomic coordinates of proteins. Nucleic Acids Res 32:W500–W502.

806 103. Bertoni M, Kiefer F, Biasini M, Bordoli L, Schwede T. 2017. Modeling protein quaternary
807 structure of homo- and hetero-oligomers beyond binary interactions by homology. Sci Rep 7.

808 104. Waterhouse A, Bertoni M, Bienert S, Studer G, Tauriello G, Gumienny R, Heer FT, de Beer
809 TAP, Rempfer C, Bordoli L, Lepore R, Schwede T. 2018. SWISS-MODEL: homology modelling of
810 protein structures and complexes. Nucleic Acids Res 46:W296–W303.

811 105. Bienert S, Waterhouse A, de Beer TAP, Tauriello G, Studer G, Bordoli L, Schwede T. 2017. The
812 SWISS-MODEL Repository—new features and functionality. Nucleic Acids Res 45:D313–D319.

813 106. Benkert P, Biasini M, Schwede T. 2011. Toward the estimation of the absolute quality of
814 individual protein structure models. Bioinformatics 27:343–350.

815 107. Guex N, Peitsch MC, Schwede T. 2009. Automated comparative protein structure modeling
816 with SWISS-MODEL and Swiss-PdbViewer: A historical perspective. Electrophoresis 30:S162–
817 S173.

818

819

820 # Figure Legends

821 **Fig. 1.** OafA and OafB are membrane bound O-acetyltransferases that acetylate the O-antigen of
822 *Salmonella*. (*A*) Schematic representation of OafA and OafB functional (coloured) and
823 transmembrane (shaded) domains predicted by InterPro and TMHMM respectively. C-term
824 constructs used for *in vitro* characterisation are indicated below the protein. (*B*) Proposed
825 mechanism of action of O-antigen acetyltransferases during maturation of the LPS in the periplasm
826 using OafA as an example. AT3 = IPR002656, SGNH= IPR013830

827 **Fig. 2.** Conservation in transmembrane domains of experimentally characterised bacterial AT3
828 carbohydrate acetyltransferases. 100% identical residues are coloured orange, similar residues in >
829 90% sequences are coloured blue, conserved small hydrophobic residues in transmembrane helices
830 were not coloured. (*A*) Conserved residues across all 30 currently known experimentally
831 characterised proteins and $OafB_{SPA}$. (*B*) Conservation in only AT3-SGNH fused proteins in the
832 alignment. See Table S1 for details of aligned sequences and Fig. S1 for full alignment.

833 **Fig. 3.** O-antigen acetylation and OafA expression from plasmid and chromosomally expressed
834 protein. (*A*) LPS immunoblot with crude LPS extracts from *Salmonella* ser. Typhimurium: LT2 basal O-
835 antigen strain expressing OafA from pBADcLIC plasmid (pWT OafA-His), LT2 WT O-antigen strain with
836 a C-terminal Deca-His tag added to the chromosomal copy of OafA (cWT OafA-His), the same strain
837 with unmodified OafA (cWT OafA), and the LT2 basal O-antigen strain with an empty pBADcLIC
838 plasmid (Empty Vector). O:5 antibody binding (Blue) shows abequose acetylation, *Salmonella* LPS
839 core antibody binding (Green) acts as a loading control. (*B*) Corresponding anti-His Western blot of
840 insoluble protein fraction for detection of His tagged OafA. Arrow indicates full length OafA protein.

841 **Fig. 4.** Summary of mutagenesis analysis of STM OafA. A diamond shape indicates residues that were
842 mutated, cysteine residues were mutated to serine and all other residues were mutated to alanine.
843 Results relate to % O-antigen acetylation compared to wild type, mutants that caused loss of protein
844 expression are diamond shaped but not coloured (G34A).

845 **Fig. 5.** Analysis of the crystal structure of $OafB_{SPA}^{C\text{-}long}$. (*A*) Cartoon representation of $OafB_{SPA}^{C\text{-}long}$ with
846 helices and sheets numbered, with the additional helix (α8) coloured teal and SGNH-extension
847 coloured orange. Catalytic residues and disulfide bonds are shown as sticks and labelled. (*B*) Surface
848 representation of $OafB_{SPA}^{C\text{-}long}$ with colouring as above and catalytic triad coloured red. (*C*) Surface
849 representation of $OafB_{SPA}^{long}$, 5UFY, 5B5S and 2VPT.

850 **Fig. 6.** Analysis of additional helix and catalytic triad residues (A*, B*) Structure based sequence
851 alignments of additional helix (A), indicated by a line above the sequence, and blocks I-V (B) with
852 residues conserved in > 50% of sequences highlighted blue, catalytic and oxyanion hole residues are
853 indicated by an arrow. Abbreviations and details of sequences used in methods section. (*C*) Catalytic
854 triad and potential oxyanion hole residues shown as sticks, hydrogen bonds to co-crystallised sulfate
855 ion shown as dashed black lines.

856 **Fig. 7.** Effect of $SGNH_{ext}$ length on substrate specificity of C-terminal OafA and OafB. Dot blot for
857 acetylated abequose (αO:5 – blue) on basal *Salmonella* ser. Typhimurium LPS after incubation with
858 purified the C-terminal OafA and OafB and pNPA as an acetyl group donor. 10 µM OafA and 20 µM
859 OafB were used in these reactions. αCore antibody (green) is used as a loading control. WT
860 acetylated LPS is used as a positive control. (+) = Active protein, (-) = Heat treated protein.
861 Representative of N=3 repeats. 'C-Long' constructs comprise the SGNH domain with full $SGNH_{ext,}$ 'C-
862 Short' constructs comprise the SGNH domain with fewer $SGNH_{ext}$ residues to expose the SGNH
863 domain active site. See Figure 1 for details of the C-terminal OafA and OafB constructs

864 **Fig. 8.** Refined model of AT3-SGNH fused O-antigen acetyltransferases. Periplasmic SGNHext
865 (Orange) is structured, therefore positioning the SGNH domain (Grey) close to the AT3 domain
866 (Purple), this orients the additional helix (Teal) in close proximity to the AT3 domain with
867 interactions between the two domains as proposed by the co-evolution analysis. These observations
868 result in the current hypothesis: 1) Cytoplasmic acetyl group donor interacts with conserved Arg in
869 TMH1, the acetyl group is processed and transferred to the periplasmic side of the inner membrane

870 and this process involves catalytic His residue of TMH1. 2) Conserved Asp and Ser mediate transfer
871 of acetate to the SGNH domain. 3) SGNH domain catalyses addition of the acetate to specific O-
872 antigen monosaccharide. The active site of the SGNH domain is highlighted by an asterisk and
873 interaction site highlighted by a "+".

874 Table Legends

875 **Table 1.** Summary of site directed mutagenesis analysis of the transmembrane domain of OafA

876 **Table 2.** Summary of site directed mutagenesis analysis of the periplasmic domain of OafA

877 Supplementary Figure Legends

878 **Fig. S1.** Alignment of characterised AT3 acetyltransferases. Protein sequences are in the same order
879 as Table S1 after *Salmonella* ser. Paratyphi A OafB WP_00400612. SGNH fused acetyltransferases are
880 indicated by a grey box. Asterisks mark residues selected for mutation from this alignment.

881 **Fig. S2.** Functional analysis of OafA membrane bound domain point mutants *in situ*. Left panel shows
882 LPS western blot with crude LPS extracts from Salmonella ser. Typhimurium basal O-antigen strain
883 expressing OafA point mutant variants in (A) the membrane domain and (B) the periplasmic domain.
884 O:5 antibody binding (Blue) shows abequose acetylation and

885

886 Salmonella LPS core antibody binding (Green) acts as a loading control. Right panel shows
887 corresponding anti-His western blot for expression of His tagged OafA. Arrow indicates full length
888 OafA protein.

889 **Fig. S3.** Structure based sequence alignment of OafB, OafA and closest structural homologues.
890 Residues conserved in >50% highlighted blue, catalytic and oxyanion hole residues are indicated by
891 an arrow. Abbreviations and details of sequences used in methods section.

892 **Fig. S4.** Melting curves of $OafA_{STM}^{C\text{-}long}$, $OafA_{STM}^{C\text{-}short}$, $OafB_{SPA}^{C\text{-}long}$ and $OafB_{SPA}^{C\text{-}short}$, with melting
893 temperatures of $OafA_{STM}^{C\text{-}long}$ = 63.8 ^{o}C, $OafA_{STM}^{C\text{-}short}$ = 58.1 ^{o}C, $OafB_{SPA}^{C\text{-}long}$ = 58.9 ^{o}C, $OafB_{SPA}^{C\text{-}short}$ =
894 50.0 ^{o}C.

895 **Fig. S5.** Comparison of potential oxyanion hole residues in OafA and OafB. A. Homology model of
896 $OafA_{STM}^{C\text{-}long}$ (yellow) modelled on the structure of OafB (grey, extension in orange and additional
897 helix in teal). Catalytic triad and potential oxyanion hole residues shown as sticks. Residues indicated
898 with OafA first. Both Ser 437 side chain and Leu 438 backbone amide are in close proximity to
899 catalytic triad and active site sulfate. B. Sequence alignment of OafA from Salmonella ser.
900 Tyhimurium and OafB from Typhimurium and Paratyphi A serovars of Salmonella from OafA residues
901 410-450. Alignments were carried out using Tcoffee with default settings. Red Box highlights
902 predicted replacements for catalytic block II glycine.

903 **Fig. S6.** In vitro acetyl-esterase activity of C-terminal OafA and OafB assessed by hydrolysis of
904 pNitrophenyl acetate (pNPA). Solid line = Active protein, dashed line = Heat treated protein. Error
905 bars = SEM, N=3. Some error bars are obscured by point markers. 'C-Long' constructs comprise the
906 SGNH domain with full SGNHext, 'C-Short' constructs comprise the SGNH domain with fewer $SGNH_{ext}$
907 residues to expose the SGNH domain active site. See Figure 1 for details of the C-terminal OafA and
908 OafB constructs.

909 **Fig. S7.** A) Predicted contact map for OafB based on a correlated mutation analysis using the RaptorX
910 webserver. The horizontal/vertical line marks residue 377, which forms the boundary at the end of
911 the AT3 domain. High confidence interactions within the AT3 domain (top left) and the SGNH
912 domain (bottom right), while a single high scoring interaction between the AT3 (93-97) and SGNH
913 (524-546) is marked (bottom left). B) Structure of $OafB_{SPA}^{C\text{-}long}$ with residues (542-546) predicted to
914 interact with the acyltransferase domain coloured blue. The extension is coloured orange, the
915 additional helix coloured teal, and catalytic triad coloured red.

916 # Supplementary Table Legends

917 **Table S1.** Experimentally characterised bacterial AT3 acetyltransferases

918 **Table S2.** Molecular biology materials. Bacterial strains and primers used in this study. Primers for
919 cloning of OafA and OafB constructs and creation of OafA point mutant variants on the
920 pBADcLIC_WT-OafA plasmid. Amp = Ampicillin 100 µg/ml, Kan = Kanamycin 50 µg/ml.

921 **Table S3.** X-ray crystallography data and statistics for the structure of $OafB_{SPA}^{C\text{-}long}$. Values in
922 parenthesis correspond to the highest resolution shell unless otherwise stated.

923

Table 1. Summary of site directed mutagenesis analysis of the transmembrane domain of OafA

Mutant	O:5 signal intensity compared to wild type % (± SEM)	Position	Reason for mutation
R14A	0.07 ± 0.04	TMH1	Specifically conserved in AT3-SGNH proteins
H25A	0.33 ± 0.18		Conserved in TMH1 across all aligned proteins
S32A	105.25 ± 30.89	Periplasmic loop & TMH2	XGG-F/Y-XGV-D/P/V-X motif found to be conserved in AT3-SGNH fused acyltransferases. In the first periplasmic loop between TMH1-2
G33A	119.17 ± 18.72		
G34A	1.36 ± 0.88*		
F35A	19.24 ± 2.70		
I36A	101.47 ± 22.72		
G37A	118.13 ± 22.11		
V38A	86.38 ± 12.73		
D39A	0.31 ± 0.07		
V40A	121.28 ± 23.82		
S45A	98.18 ± 24.30	TMH2	Conserved in SG in TMH2
G46A	99.59 ± 22.01		
R69A	0.10 ± 0.04	TMH3	RXXR motif previously identified as critical for function
R72A	0.07 ± 0.02		
S112A	0.24 ± 0.09	TMH3-4 Periplasmic loop	Conserved in periplasmic loop between TMH3-4 in AT3-SGNH fused proteins
N113A	93.79 ± 14.92		
Y122A	85.76 ± 7.58		
G202A	74.14 ± 10.70	TMH6	Conserved trans membrane glycine
E325A (Linker)	4.84 ± 1.13	TMH10-11 Cytoplasmic loop	Conserved after TMH10 in all AT3-SGNH fused proteins

Dark Grey= Point mutants with <1% O:5 signal intensity, Light Grey = Point mutants with <50% O:5 signal intensity, * = No OafA protein expression detected. Values represent the average of 2 biological repeats with 3 technical replicates.

Table 2. Summary of site directed mutagenesis analysis of the periplasmic domain of OafA

Mutant	O:5 signal intensity compared to wild type % (± SEM)	Reason for mutation
C383,397S (Linker)	107.40 ± 26.80	Conserved disulphide bonding pairs
C439,453S	185.06 ± 54.63	
C567,572S	49.98 ± 4.33	
S437A	45.59 ± 3.42	Potential oxyanion hole residue
E569A	99.87 ± 7.01	Conserved between most C-term Cys pair
S412A	0.36 ± 0.26	SGNH domain catalytic triad residues
D587A	10.13 ± 1.70	
H590A	0.87 ± 0.62	

Dark Grey= Point mutants with <1% O:5 signal intensity, Light Grey = Point mutants with <50% O:5 signal intensity. Values represent the average of 2 biological repeats with 3 technical replicates.

Figure 1

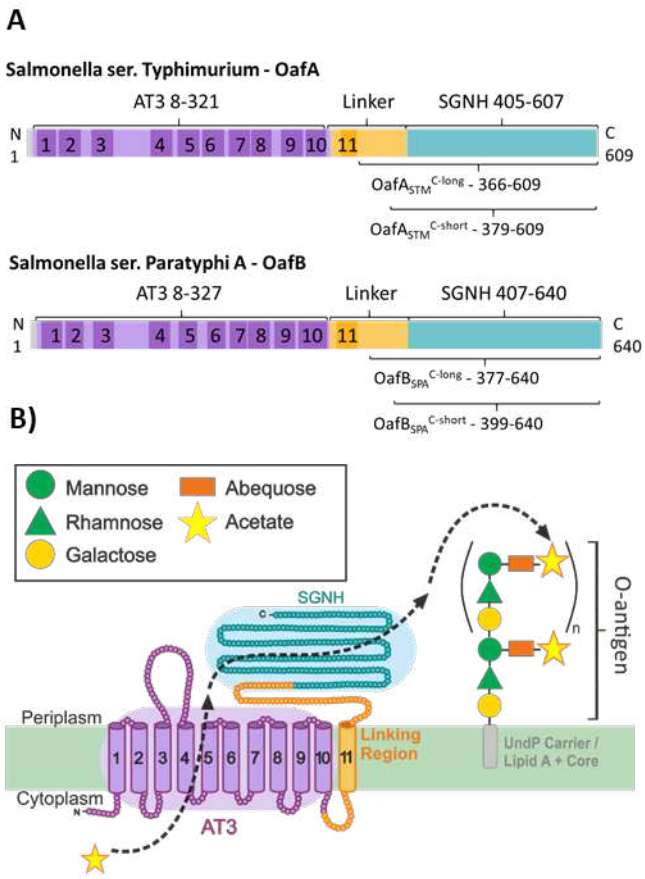
A
Salmonella ser. Typhimurium - OafA
AT3 8-321
Linker
SGNH 405-607
N
1
1 2 3 4 5 6 7 8 9 10 11
C
609
OafA$_{STM}^{C\text{-}long}$ - 366-609
OafA$_{STM}^{C\text{-}short}$ - 379-609
Salmonella ser. Paratyphi A - OafB
AT3 8-327
Linker
SGNH 407-640
N
1
1 2 3 4 5 6 7 8 9 10 11
C
640
OafB$_{SPA}^{C\text{-}long}$ - 377-640
OafB$_{SPA}^{C\text{-}short}$ - 399-640
B)
Mannose
Abequose
Rhamnose
Acetate
Galactose
SGNH
O-antigen
n
Periplasm
Cytoplasm
1 2 3 4 5 6 7 8 9 10 11
Linking Region
UndP Carrier / Lipid A + Core
AT3

Figure 2

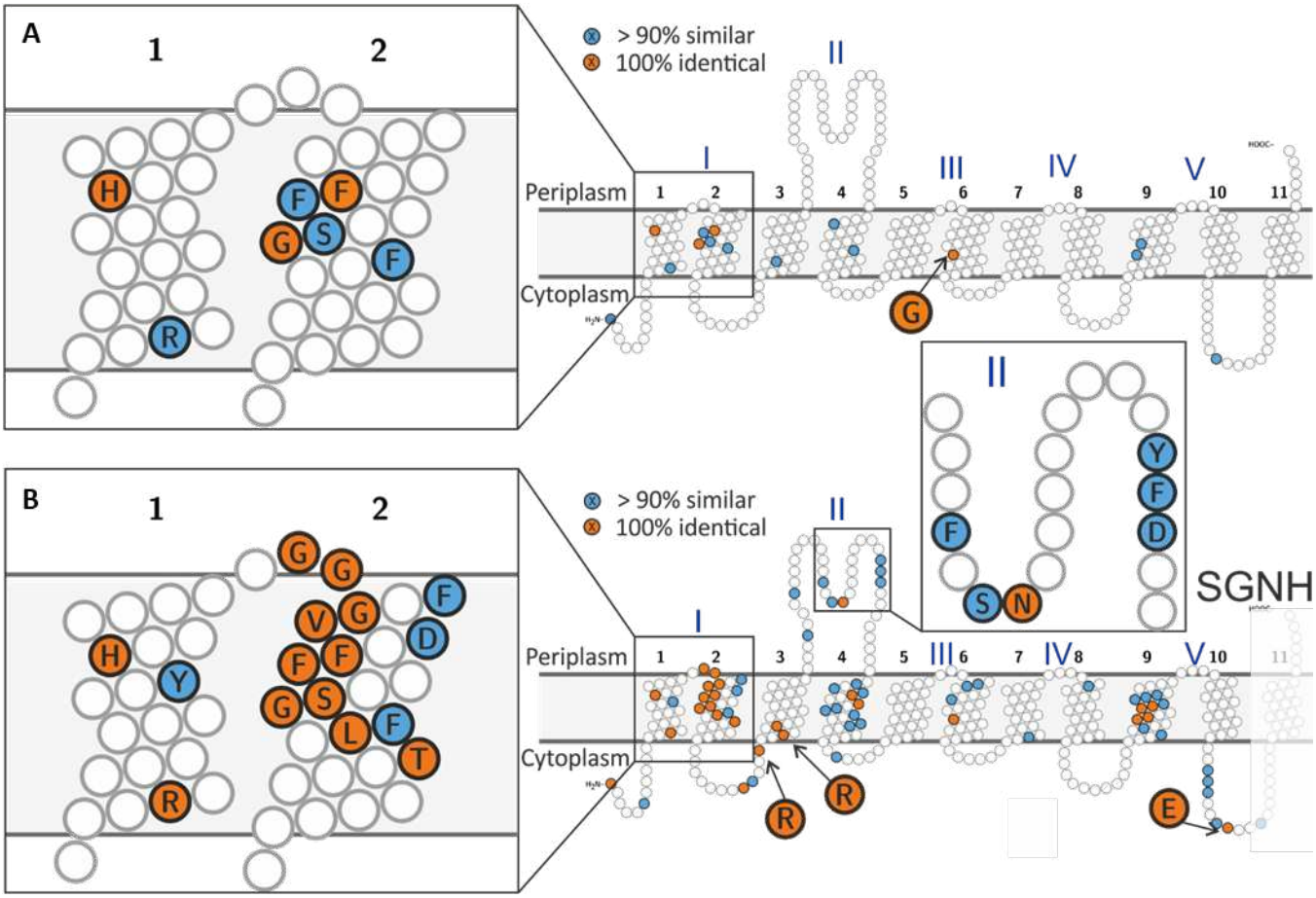
A
1
2
H
F
F
G
S
F
R
> 90% similar
100% identical
II
I
III
IV
V
Periplasm
Cytoplasm
1
2
3
4
5
6
7
8
9
10
11
G
II
Y
F
D
F
S
N
SGNH
B
1
2
G
G
F
V
G
D
H
F
F
Y
G
S
L
F
T
R
> 90% similar
100% identical
II
I
III
IV
V
Periplasm
Cytoplasm
1
2
3
4
5
6
7
8
9
10
11
R
R
E

Figure 3

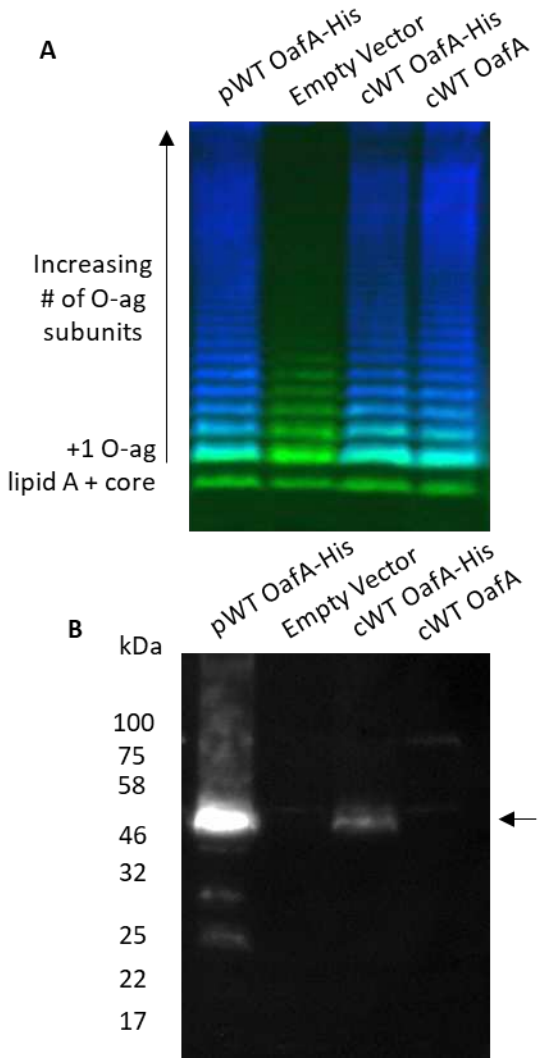
A
pWT OafA-His
Empty Vector
cWT OafA-His
cWT OafA
Increasing
# of O-ag
subunits
+1 O-ag
lipid A + core
B
kDa
pWT OafA-His
Empty Vector
cWT OafA-His
cWT OafA
100
75
58
46
32
25
22
17

Figure 4

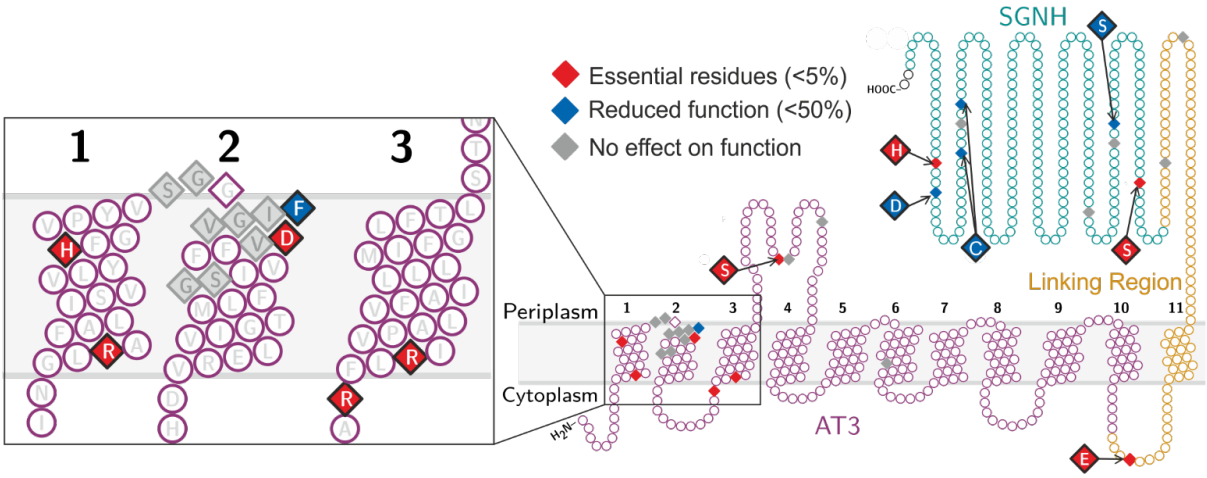
1
2
3
Essential residues (<5%)
Reduced function (<50%)
No effect on function
SGNH
HOOC
Linking Region
Periplasm
Cytoplasm
1
2
3
4
5
6
7
8
9
10
11
AT3
H2N

Figure 5

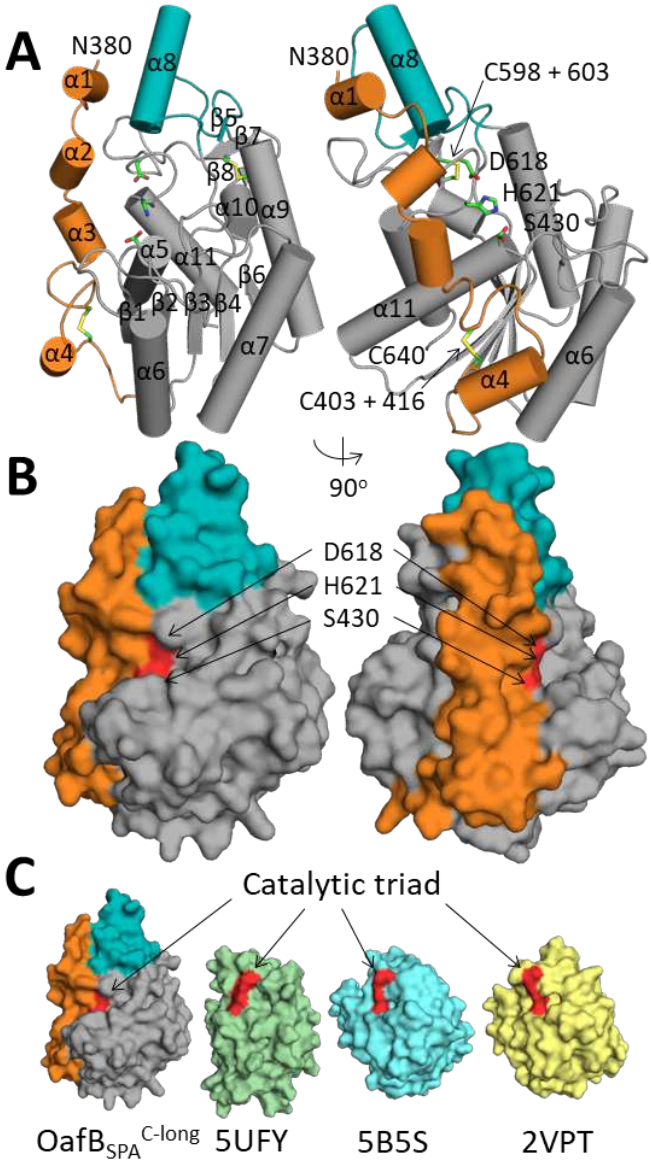
A
N380
α1
α8
α2
β5
β7
β8
α10
α9
α3
α5
α11
β6
β1
β2
β3
β4
α4
α6
α7
N380
α8
α1
C598 + 603
D618
H621
S430
α11
C640
α4
α6
C403 + 416
90°
B
D618
H621
S430
C
Catalytic triad
OafB$_{SPA}^{C\text{-}long}$
5UFY
5B5S
2VPT

Figure 6

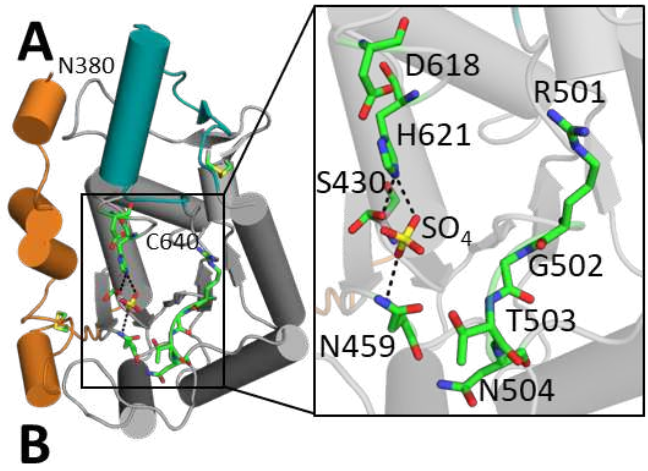

Additional helix

```
OafB-S.PA     535  ........WNANLVKIISNYLSEFKKTPPLYMTYGLNSEI  575
OafB-S.Tym    535  ........WNANLVKVISNYTSEFKKTPPIYMSYGLNDEI  575
OafA-S.Tym    505  .........KKTMIDTIEDMGINSGRTVPWSM.TDETRNL  544
OafA-H.inf    514  .......SPL...RGYLLENYGLEKYLTPI....HRMGDI  551
OatA-S.pne    516  ........DKT......................KETYAIV  534
OatA-S.aur    530  ......................................DYE  542
Ape1-N.men    285  TLGVCGTRPV...........................RL  308
TAP1-E.col    131  .......GRR...........................YN  147
RGAE-A.acu    131  .......ETGTFVN......................SP  151
5B5S-T.cel    127  ....................................DATI  142
2VPT-C.the    129  ....................................AI  141
```

C

Block I

```
OafB-S.PA     425  FIIGDSYAAA  434
OafB-S.Tym    425  FIIGDSYAAA  434
OafA-S.Tym    407  VVWGDSHAAH  416
OafA-H.inf    405  IILGDSHSSH  414
OatA-S.pne    433  MLIGDSVALR  442
OatA-S.aur    448  LLIGDSVMVD  457
Ape1-N.men     57  LQIGDSHTAG   66
TAP1-E.col     31  LILGDSLSAG   40
RGAE-A.acu      4  YLAGDSTMAK   13
5B5S-T.cel      5  MLLGDSITEI   14
2VPT-C.the      7  MPVGDSCTEG   16
```

Block II

```
455  MTD.....GNAPPLFV  465
455  MTD.....GNAPPLFV  465
434  RTASLCPPIIGLQKDD  449
435  DKFECSFIVN.EQYQL  449
457  NAQ.....VS......  461
472  DGK.....VG......  476
214  MGI.....NG......  218
66   ASI.....SG......  70
38   DAV.....AG......  42
58   EGH.....SG......  62
63   EGH.....SG......  67
```

Block III

```
OafB-S.PA     498  WSV..RGTNG...VHD  508
OafB-S.Tym    498  WSV..RGSNG...VHD  508
OafA-S.Tym    476  ALWPVY..........  481
OafA-H.inf    476  MGGQPVPRFRPETFIE  491
OatA-S.pne    488  TGVNNPE.........  494
OatA-S.aur    504  LGINGAFTK.......  512
Ape1-N.men    247  YGTNEAFNNNID....  258
TAP1-E.col     96  LGGNDGLRG....FQP  107
RGAE-A.acu     71  FGHNDGGSLS...TDN   83
5B5S-T.cel     89  LGTNDVNIGH...RNA  101
2VPT-C.the     93  IGGNDLLLNG......  102
```

Block V

```
615  TAVDWGHL..  622
615  TAVDWGHL..  622
585  .QYDNAHL..  591
587  .YGDQDHL..  593
565  AGTDQVHFGS  574
573  .AYDGIHL..  579
346  .AKDGVHF..  352
178  .QDDGIHP..  184
190  .PIDHTHT..  196
177  .RDDGVHP..  183
176  .SWDGLHL..  182
```

Figure 7

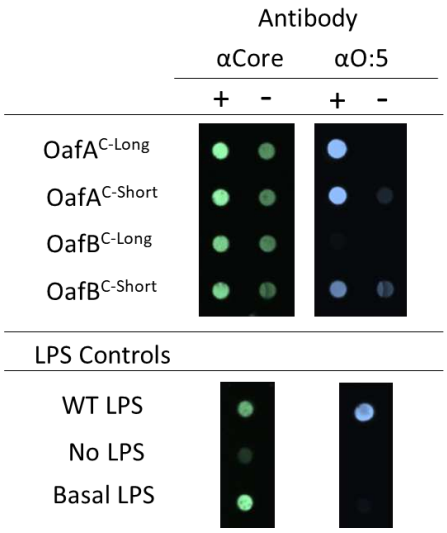
Antibody
αCore
αO:5
+
-
+
-
OafA C-Long
OafA C-Short
OafB C-Long
OafB C-Short
LPS Controls
WT LPS
No LPS
Basal LPS

Figure 8

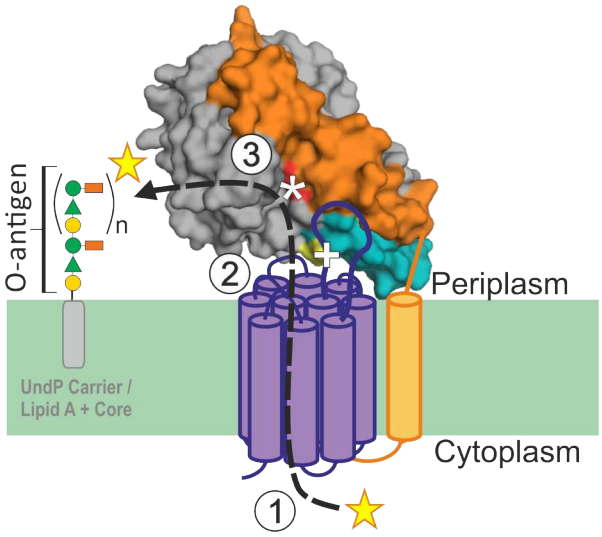
O-antigen
n
3
2
1
Periplasm
Cytoplasm
UndP Carrier /
Lipid A + Core